

RESEARCH ARTICLE

Interaction of the human erythrocyte Band 3 anion exchanger 1 (AE1, SLC4A1) with lipids and glycophorin A: Molecular organization of the Wright (Wr) blood group antigen

Antreas C. Kalli^{1,2*}, Reinhart A. F. Reithmeier³

1 Leeds Institute of Cancer and Pathology, University of Leeds, Leeds, United Kingdom, **2** Astbury Centre for Structural Molecular Biology, University of Leeds, Leeds, United Kingdom, **3** Department of Biochemistry, University of Toronto, Toronto, Canada

* a.kalli@leeds.ac.uk



OPEN ACCESS

Citation: Kalli AC, Reithmeier RAF (2018) Interaction of the human erythrocyte Band 3 anion exchanger 1 (AE1, SLC4A1) with lipids and glycophorin A: Molecular organization of the Wright (Wr) blood group antigen. *PLoS Comput Biol* 14(7): e1006284. <https://doi.org/10.1371/journal.pcbi.1006284>

Editor: Roland L. Dunbrack, Jr., Fox Chase Cancer Center, UNITED STATES

Received: December 21, 2017

Accepted: June 8, 2018

Published: July 16, 2018

Copyright: ©2018 Kalli, Reithmeier. This is an open access article distributed under the terms of the [Creative Commons Attribution License](https://creativecommons.org/licenses/by/4.0/), which permits unrestricted use, distribution, and reproduction in any medium, provided the original author and source are credited.

Data Availability Statement: All relevant data are within the paper and its Supporting Information files.

Funding: ACK was supported by a Springboard Award from the Academy of Medical Sciences (GB) and the Wellcome Trust [Grant number: SBF002 \1031]. This research was enabled in part by support provided by Scinet (<https://www.scinethpc.ca>) and Compute Canada (www.computecanada.ca). The funders had no role in

Abstract

The Band 3 (AE1, SLC4A1) membrane protein is found in red blood cells and in kidney where it functions as an electro-neutral chloride/bicarbonate exchanger. In this study, we have used molecular dynamics simulations to provide the first realistic model of the dimeric membrane domain of human Band 3 in an asymmetric lipid bilayer containing a full complement of phospholipids, including phosphatidylinositol 4,5-bisphosphate (PIP₂) and cholesterol, and its partner membrane protein Glycophorin A (GPA). The simulations show that the annular layer in the inner leaflet surrounding Band 3 was enriched in phosphatidylserine and PIP₂ molecules. Cholesterol was also enriched around Band 3 but also at the dimer interface. The interaction of these lipids with specific sites on Band 3 may play a role in the folding and function of this anion transport membrane protein. GPA associates with Band 3 to form the Wright (Wr) blood group antigen, an interaction that involves an ionic bond between Glu658 in Band 3 and Arg61 in GPA. We were able to recreate this complex by performing simulations to allow the dimeric transmembrane portion of GPA to interact with Band 3 in a model membrane. Large-scale simulations showed that the GPA dimer can bridge Band 3 dimers resulting in the dynamic formation of long strands of alternating Band 3 and GPA dimers.

Author summary

Human Band 3 (AE1, SLC4A1), an abundant 911 amino acid glycoprotein, catalyzes the exchange of bicarbonate and chloride across the red blood cell membrane, a process necessary for efficient respiration. Malfunction of Band 3 leads to inherited diseases such as Southeast Asian Ovalocytosis, hereditary spherocytosis and distal renal tubular acidosis. Despite much available structural and functional data about Band 3, key questions about the conformational changes associated with transport and the molecular details of its interaction with lipids and other proteins remain unanswered. In this study, we have used

study design, data collection and analysis, decision to publish, or preparation of the manuscript.

Competing interests: The authors have declared that no competing interests exist.

computer simulations to investigate the dynamics of Band 3 in lipid bilayers that resemble the red blood cell plasma membrane. Our results suggest that negatively charged phospholipids and cholesterol interact strongly with Band 3 forming an annulus around the protein. Glycophorin A (GPA) interacts with Band 3 to form the Wright (Wr) blood group antigen. We were able to recreate this complex and show that GPA promotes the clustering of Band 3 in red blood cell membranes. Understanding the molecular details of the interaction of Band 3 with GPA has provided new insights into the nature of the Wright blood group antigen.

Introduction

Band 3, the human erythrocyte anion exchanger 1 (AE1, SLC4A1) is responsible for the rapid electro-neutral exchange of chloride and bicarbonate across the plasma membrane; a process that increases the blood's capacity to carry carbon dioxide as plasma bicarbonate [1]. Human Band 3 is a 911 amino acid glycoprotein consisting of a N-terminal cytosolic domain (cdAE1, residues 1–360) responsible for the interaction with the cytoskeleton [2] and a C-terminal membrane domain (mdAE1, residue 361–911) responsible for its transport function [3,4]. Band 3 is predominantly a dimer in the membrane and when isolated in detergent solutions [5,6]. The isolated cdAE1 is also a dimer [7] as is the mdAE1 [8–10]. The crystal structure of the human mdAE1 was reported in 2015 [11]. Each subunit consists of 14 transmembrane (TM) segments arranged in an inverted 7 + 7 topology (Fig 1) in agreement with most topology studies [12–20]. The bacterial UraA proton-coupled uracil transporter [21], a bacterial SLC26 fumarate transporter [22], and a fungal proton-purine symporter, UapA [23] have a similar 7 + 7 inverted repeat topology creating a novel class of seven transmembrane segment inverted repeat carriers [24]. Each monomer consists of two sub-domains with TM1, 2, 3, 4 and TM8, 9, 10, 11 coming together to form a core domain and TM5, 6, 7 and TM12, 13 and 14 to form a gate domain (Fig 1). It is the relative movement of these two sub-domains that provides the alternating access to the central anion binding site [25]. The molecular details of this movement have yet to be established, likely operating in rocker-switch or elevator mode [26–28]. The dimer is held together by a central 4-helix bundle with predominant interactions at the extra-cellular ends of TM5 and 6, however there is significant space in the dimer interface of the crystal structure. It is unclear why the 4-helix bundle is not more tightly packed or if the dimer interface is dynamic.

The native mdAE1 was produced by limited proteolysis of red cell ghosts prepared from intact erythrocytes pretreated with the anion transport inhibitor H₂DIDS [29,30]. This inhibitor reacts covalently with Lys539 and Lys851 within the gate domain, crosslinking two parts of the protein together and locking it into an outward-facing conformation [31]. The presence of the inhibitor is known to stabilize the protein against thermal denaturation [32–34]. The crystals were formed using a Fab fragment [35] in the presence of dodecylmaltoside, a commonly-used detergent known to stabilize Band 3 [36,37]. While the recent crystal structure of mdAE1, albeit static, can provide significant new insights into the Band 3 function, it does not include its native lipid environment. One purpose of our simulations was to determine the structure of mdAE1 in the absence of antibody and the H₂DIDS inhibitor in a lipid bilayer rather than in a detergent micelle. Similar MD simulations of the bacterial UraA uracil transporter revealed specific interactions with lipids and an intermediate closed state in the absence of substrate [38].

Additionally, it has been shown that Band 3 function may be regulated by lipids [39–46]. The second purpose of our simulations was to assemble the dimeric mdAE1 into an

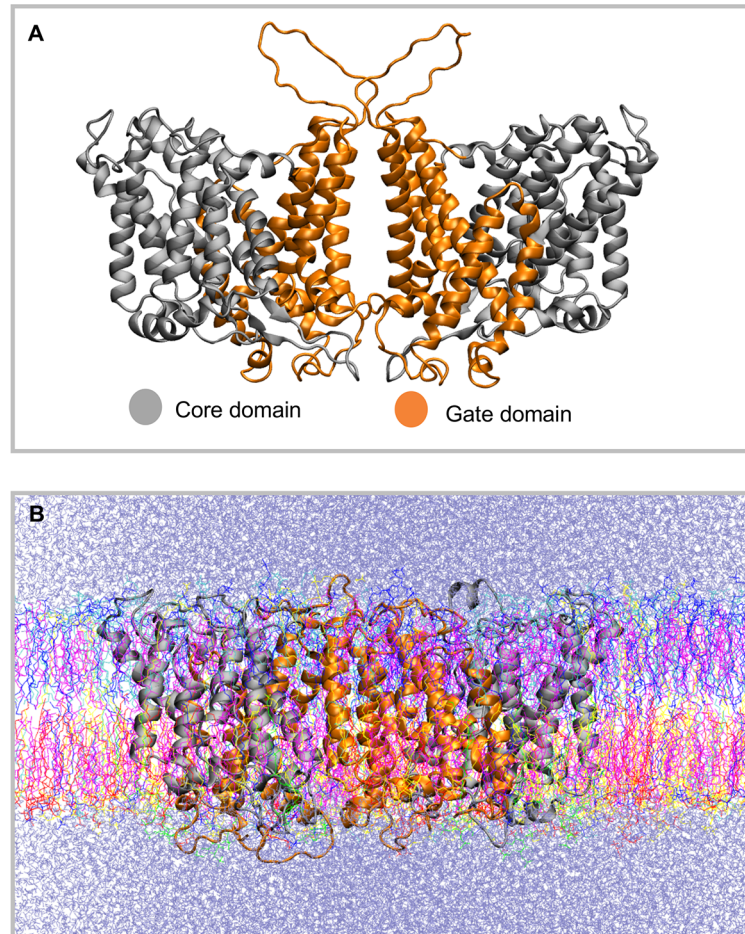


Fig 1. Band 3 structure. A. Structure of the dimeric Band 3 membrane domain (mdAE1) that was used in our simulations. The mdAE1 core domain is shown in grey and the gate domain in orange. Note that some unstructured regions that are missing from the crystal structure (PDB: 4YZF) have been modelled. B. Snapshot from the end of one of the atomistic simulations in which mdAE1 is embedded in a complex asymmetric bilayer (Band3_AT-1). The different lipid types are shown in different colors and the water is shown in ice-blue.

<https://doi.org/10.1371/journal.pcbi.1006284.g001>

asymmetric lipid bilayer containing cholesterol and other phospholipids to mimic the native red cell membrane. Fluorescence digital imaging showed that Band 3 is localized to PC-rich domains of erythrocyte membranes and is excluded from PS-rich domains [47]. In the erythrocyte membrane, pyrene-labelled phosphoinositides preferentially associate with Band 3 compared to PC [48]. Reconstitution experiments showed that transport activity of purified AE1 is sustained in the presence of PC and PE, but is inhibited by enriched levels (beyond 30 mole %) of PS [39]. Head groups also affect Band 3 stability with PE and PC stabilizing the protein while acidic lipids PG and PS destabilizing the protein. EPR measurements on ghost membranes indicated a strong interaction of spin-labelled cholesterol with Band 3 [45]. Enriched levels of cholesterol in erythrocytes decreased anion transport activity perhaps by restricting the conformational change in Band 3 that occurs during transport [49]. Band 3 interacts strongly with cholesterol and is proposed to contain a high affinity inhibitory cholesterol-binding site [44,46]. No tightly-associated lipid or detergent molecules were however resolved in the 3.5Å crystal structure of mdAE1. While collectively all these data suggest that lipids play a major

role in Band 3 function, the molecular details of the Band 3/lipid interactions remain largely unknown, a knowledge gap that can be filled by computational studies.

Glycophorin A (GPA) is known to interact with AE1 in the endoplasmic reticulum (ER) and to promote Band 3 trafficking to the cell surface [50–53]. Anion transport is impaired in red cells devoid of glycophorin A [54,55]. In the mature erythrocyte the GPA/Band 3 complex forms the Wright (Wr) blood group antigen [56]. This interaction involves the specific interaction of Glu658 in Band 3 with Arg61 in GPA [56]. A Glu658Lys mutation creates the Wrb antigen perhaps due to the dissociation of the complex, although this has not been established. In the mdAE1 structure Glu658 is located in the extracellular loop connecting TM7 and TM8 on the periphery of the structure far away from the dimer interface. Despite the fact that the structures of both the mdAE1 and TM portion of GPA are available, no structure of the mdAE1/GPA complex exists and also the molecular details of this complex or its dynamics are largely unknown.

Using MD simulations, we created a dynamic model of mdAE1 in a native membrane and studied its interaction with lipids, and with GPA. We discovered that certain basic residues had specific interactions with inner leaflet acidic phospholipids phosphatidylserine and PIP₂. Cholesterol was also enriched in the annular lipids surrounding the protein, but also at the dimer interface. We demonstrate that GPA association with mdAE1 occurs not only via an interaction of Arg61 with Glu658 but also via additional interactions of the TM and extracellular part of GPA with Band 3. Finally, large-scale simulations showed that the GPA dimer could sequentially bridge mdAE1 dimers creating alternating strands of these two proteins in a lipid bilayer. The MD simulations provide the first dynamic model of Band 3 in a complex lipid bilayer and molecular details about the interaction of Band 3 with lipids and with GPA.

Results

Interaction of Band 3 with anionic lipids

To study the interaction of the mdAE1 dimer with the different lipids that are present in the erythrocyte plasma membrane, the 1-palmitoyl-2-oleoyl-phosphatidylcholine (POPC) lipids that were self-assembled around mdAE1 (see [1]) were exchanged with other lipids using a computer script [57] to create an asymmetric bilayer containing 45% POPC and 5% 1-palmitoyl-2-oleoyl-phosphatidylethanolamine (POPE) in the outer leaflet and 12% POPC, 23% POPE, 15% 1-palmitoyl-2-oleoyl-phosphatidylserine (POPS) in the inner leaflet. Note that in these simulations the H₂DIDS molecule present in the mdAE1 crystal structure was removed, as was the antibody used for crystallization. Five independent simulations of 10 μs each were performed. Analysis of the lipid density around the protein revealed a high density of POPS lipids around mdAE1 (Fig 2A). Indeed, during the simulations a discontinuous anionic annulus is formed around mdAE1 in the inner bilayer leaflet. Analysis of the interactions between mdAE1 and POPS lipids showed that the POPS head groups interact predominantly with positively charged Lys and Arg residues on the mdAE1 surface. The residues that form the highest number of contacts are at positions R387, R514, K600, K826, T830, W831, R832, H834 and R879.

To study further the interactions between lipids and mdAE1 and how this may be affected by other lipids, including PIP₂ and cholesterol, we have also run simulations of mdAE1 in increasing complex bilayers. In particular, we have constructed seven different bilayers of increasing complexity with lipids that are found in the red blood cell membrane (see Table 1). In all cases the anionic annulus around mdAE1 was retained. The contact positions of PIP₂, POPS and POPE around Band 3 are shown in S1 Fig. The preferential interactions of POPS lipids were reduced in certain areas around mdAE1 when PIP₂ lipids were present in our simulations (Fig 2B and 2C). The red blood cell plasma membrane contains a small percentage

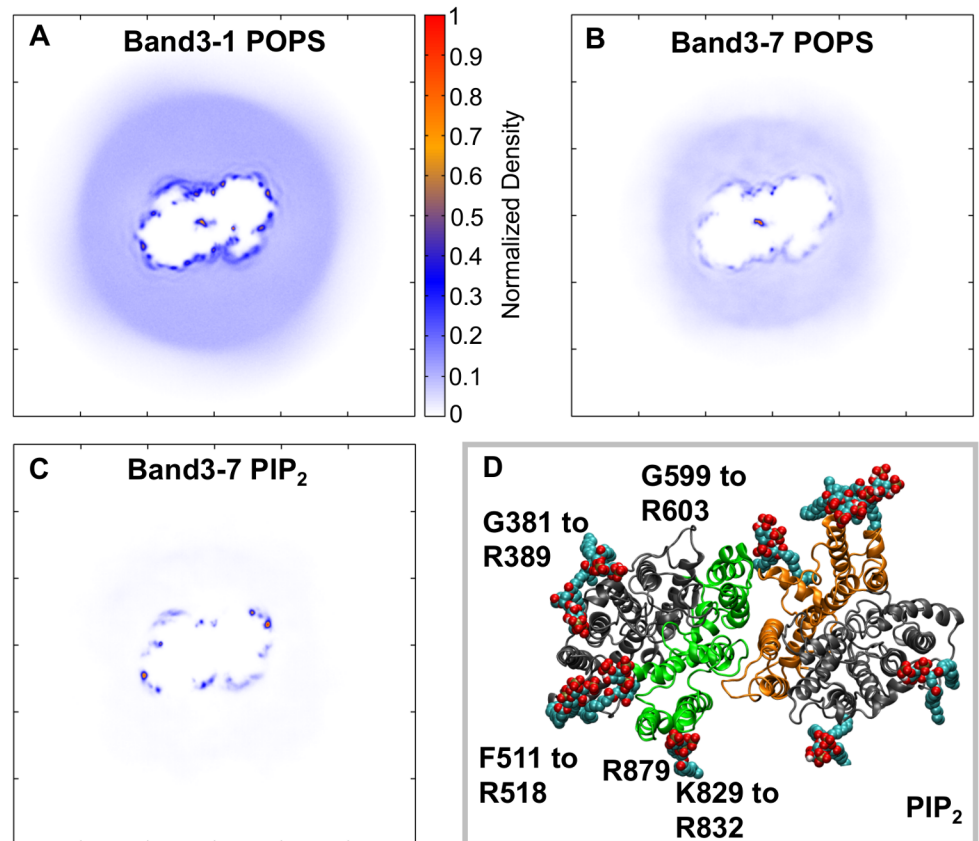


Fig 2. Interaction of Band 3 with anionic lipids. A,B,C. Two-dimensional density of POPS (A, B) and PIP₂ (C) molecules around Band 3 in the bilayer inner leaflet. The density in A was calculated using all repeat simulations of the Band3-1 (i.e. without PIP₂) system and the densities in B and C were calculated using all repeat simulations of the Band3-7 system (see Table 1). D. Snapshot from the end of one of the atomistic simulations showing the interactions of mdAE1 dimer with PIP₂ lipids. See also S1 and S2 Figs.

<https://doi.org/10.1371/journal.pcbi.1006284.g002>

(~2%) of PIP lipids in the inner leaflet. Despite the small number of PIP₂ molecules in our simulation, the discontinuous anionic annulus around mdAE1 was formed mainly by PIP₂ lipids and not POPS (Fig 2). Additionally, the PIP₂ lipids were more specifically-localized in their interactions compared to POPS lipids. PIP₂ molecules mainly interacted with the regions comprised of residues G381 to R389, R514, G599 to R603, H703, K826, K829 to R832, and R879. The dimeric nature of mdAE1 allowed the comparison of the lipid interactions in the two subunits, providing a built-in replicate. Indeed, both subunits exhibited similar pattern of lipid interactions (Fig 2).

The strong interactions of PIP₂ molecules with mdAE1 also reduced the diffusion of the PIP₂ molecules compared to the other lipids in our systems. In the Band3-6 (Table 1) simulations in which PIP₂ molecules were part of the bilayer, the diffusion coefficient of all PIP₂ lipids is $0.51 \pm 0.07 \times 10^{-7} \text{ cm}^2/\text{s}$ (linear diffusion). The diffusion coefficients for POPC, POPE and POPS lipids is $1.28 \pm 0.06 \times 10^{-7} \text{ cm}^2/\text{s}$, $1.04 \pm 0.06 \times 10^{-7} \text{ cm}^2/\text{s}$, $0.92 \pm 0.09 \times 10^{-7} \text{ cm}^2/\text{s}$, respectively. The reduced diffusion of PIP₂ lipids possibly is due to their strong interactions with the protein. A similar trend occurs in the Band3-7 simulation in which we have PIP₂ lipids and sphingomyelin. We note that the diffusion of all lipids reduces as we increase the concentration of cholesterol. For example, the POPC diffusion in the system with no cholesterol is $5.89 \pm 0.06 \times 10^{-7} \text{ cm}^2/\text{s}$, compared to $1.28 \pm 0.06 \times 10^{-7} \text{ cm}^2/\text{s}$ in the systems we have the native 50% level of cholesterol.

Table 1. Summary of simulations with Band 3.

Simulation	Composition Outer leaflet	Composition Inner leaflet	Duration
<i>Coarse-grained:</i>			
<i>Band3-1</i>	POPC:POPE (~45:5)	POPC:POPE:POPS (~12:23:15)	5 x 10 μ s
<i>Band3-2</i>	POPC:POPE:CHOL (~42.5:5:2.5)	POPC:POPE:POPS:CHOL (~11.5:21.5:14.5:2.5)	5 x 10 μ s
<i>Band3-3</i>	POPC:POPE:CHOL (~41:4:5)	POPC:POPE:POPS:CHOL (~11:20:14:5)	5 x 10 μ s
<i>Band3-4</i>	POPC:POPE:CHOL (~30:7.5:12.5)	POPC:POPE:POPS:CHOL (~9.5:16:12:12.5)	5 x 10 μ s
<i>Band3-5</i>	POPC:POPE:CHOL (~22.5:2.5:25)	POPC:POPE:POPS:CHOL (~6:11.5:7.5:25)	5 x 10 μ s
<i>Band3-6</i>	POPC:POPE:CHOL (~22.5:2.5:25)	POPC:POPE:POPS:PIP ₂ :CHOL (~6:11.5:6.5:1:25)	5 x 10 μ s
<i>Band3-7</i>	POPC:SM:POPE:CHOL (~11.5:11:2.5:25)	POPC:SM:POPE:POPS:PIP ₂ :CHOL (~4:2:11.5:6.5:1:25)	5 x 10 μ s
<i>Band3-8</i>	POPC:SM:POPE:CHOL (~21.5:21:5:2.5)	POPC:SM:POPE:POPS:CHOL (~7.5:4:21.5:14.5:2.5)	5 x 10 μ s
<i>Atomistic:</i>			
<i>Band3_AT-1</i>	POPC:SM:POPE:CHOL (~11.5:11:2.5:25)	POPC:SM:POPE:POPS:PIP ₂ :CHOL (~4:2:11.5:6.5:1:25)	3 x 250 ns
<i>Band3_AT-2</i>	POPC:POPE (~45:5)	POPC:POPE:POPS (~12:23:15)	3 x 250 ns

<https://doi.org/10.1371/journal.pcbi.1006284.t001>

Cholesterol interactions with AE1

The red blood cell plasma membrane consists of a high concentration of cholesterol (~50% of lipids), which may regulate the function of AE1. To study the interactions of Band 3 with cholesterol we have run simulations of the mdAE1 dimer in bilayers with increasing concentration of cholesterol (5%, 10%, 25% and 50%). Cholesterol showed a preferential interaction with mdAE1 regardless of its concentration in the membrane (Fig 3). Increasing the cholesterol concentration increased the number of cholesterol molecules surrounding mdAE1. Analysis of the radial density of cholesterol showed an enrichment of cholesterol in most parts of the annular layer surrounding mdAE1 at 5% cholesterol and this enrichment did not change upon increasing the cholesterol concentration to 10%, 25% and 50%. Interactions of cholesterol with mdAE1 were rather dynamic and cholesterol could be seen to “flip-flop” across the membrane during the simulation, a process observed with native erythrocytes [58]. Analysis of the interactions between the cholesterol hydroxyl group and mdAE1 suggested residues V383, F401, S438, I442, F515, F544, K600, I624, L775, H834 and R871 made the largest number of interactions with the cholesterol hydroxyl head group (Fig 3 and S1D Fig). Interestingly, cholesterol is also bound in the dimer interface (Fig 3A and 3B). In the mdAE1 crystal structure there is a cavity in the dimer interface that in our simulations is filled mainly with cholesterol.

Atomistic simulations

In order to study the interactions between the lipids and mdAE1 in molecular detail, snapshots from 3 different coarse-grained simulations (from the Band3-7 system; Table 1) were converted to atomistic representations and further simulations of 250 ns were performed. The conversion was done as described in [59]. Calculation of the interactions between PIP₂ and mdAE1 suggests that the interactions observed in our coarse-grained simulations above were retained (S3A Fig). In the atomistic simulations, residues L382 to R384, R387, K600 and K829 to R832 made the highest number of interactions with PIP₂ lipids. Cholesterol was bound at sites that commonly contained an aromatic residue. In the atomistic simulations, the polar hydroxyl group of cholesterol made significant interactions with residues Y390, Y393, A400 to S402, F511, F515, Q545, K600, W648, W662 and H834 (S3B Fig).

Comparison of the protein structures at the end of our atomistic simulations with the mAE1 crystal structure reveals a significant fluctuation in the position of TM helices 13, 14

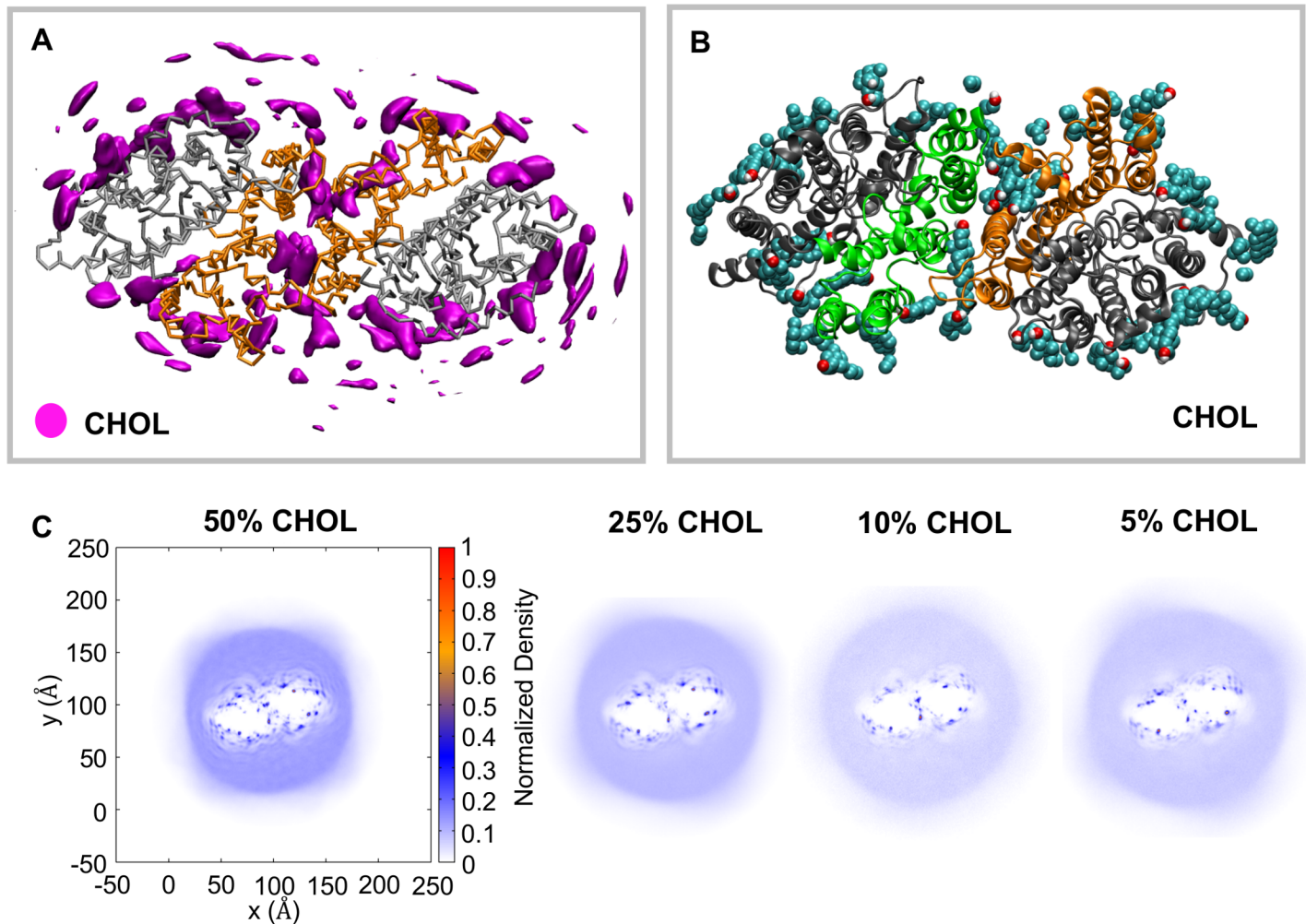


Fig 3. Interactions of Band 3 with cholesterol. A. Average density of cholesterol around mdAE1. The density was calculated using all repeat simulations of the Band3-7 system (see Table 1). B. Snapshot from the end of one of the simulations showing the interactions of mdAE1 dimer with cholesterol. C. Two-dimensional density of the cholesterol around mdAE1. Different systems are shown that contain different concentration of cholesterol. The normalization was done by dividing the number of lipids in each bin with the number of frames and the bin area. After the density calculation, the density was divided by the largest density and thus the highest density region has a value of 1. See also S1 Fig.

<https://doi.org/10.1371/journal.pcbi.1006284.g003>

and H6. The movement of those helices varied between the simulation repeats (Fig 4A and 4B). Additionally, a small shift of helix 5 of the gate domain towards the core domain is observed in most simulations (Fig 4B). Interestingly, no major changes within the core domain were observed with the exception of helix 3, which shifts towards the gate domain. These changes in the helices resulted in structures that in most simulations are still in an outward-open conformation but the opening in the extracellular region is narrower. We note that some of the changes in the position of helices 13, 14 and H6 were observed during the coarse-grained simulations. Additionally, in some of the simulations, some of the helicity of H1 is lost. Similar changes within the domains were observed in atomistic simulations in which snapshots of the Band3-1 systems (i.e. without any cholesterol) were performed. In this case however, a change in helix 3 position was observed only in one of the simulations.

In the crystal structure H₂DIDS crosslinked K539 in TM5 to K851 that is located at the end of helix 13. The side chain of K851 still points towards the core domain in our simulations,

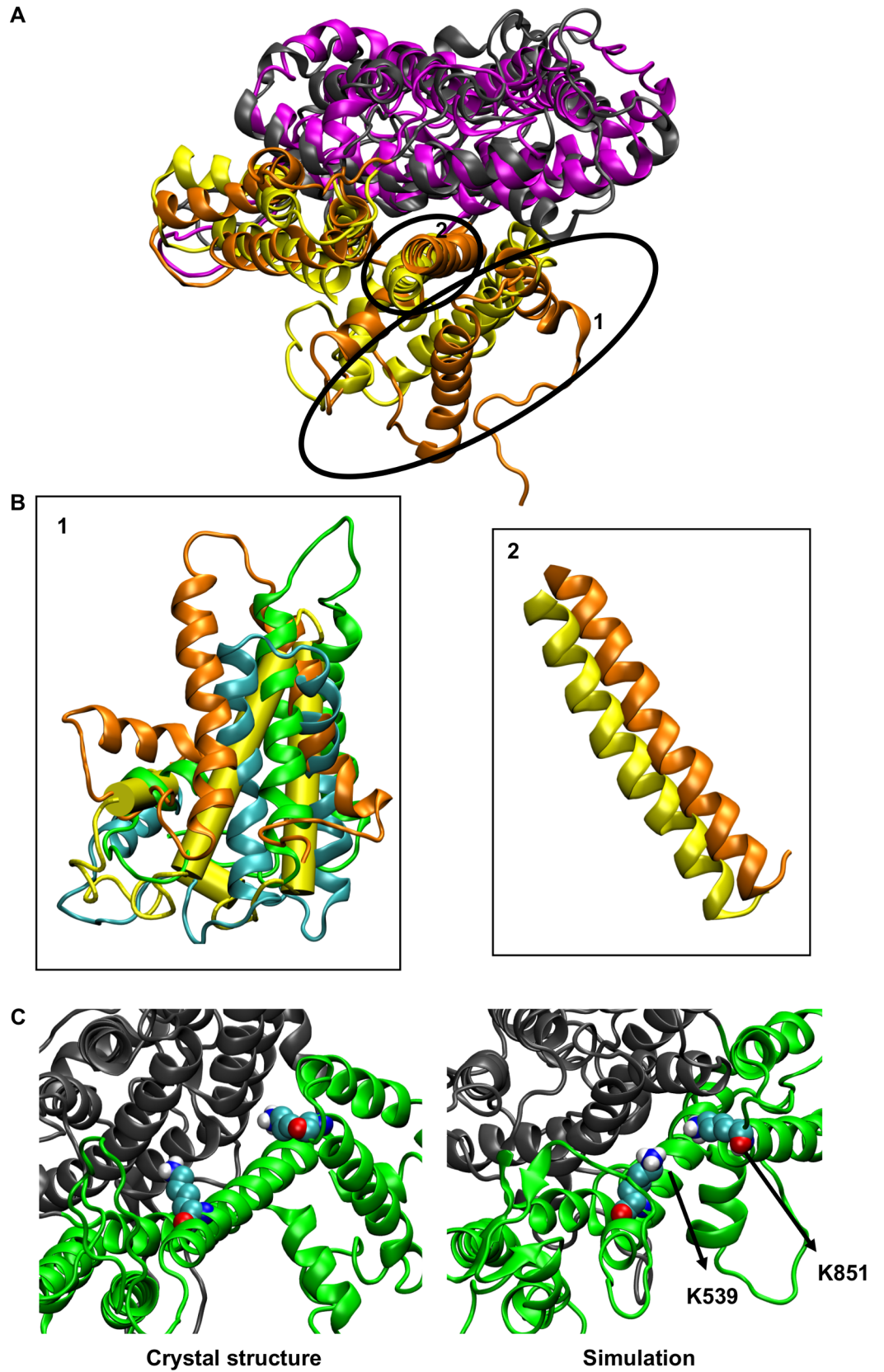


Fig 4. Atomistic simulations of Band 3. A. Alignment of the helical regions of the core domain, with the exception of helix 3, of a Band 3 monomer from Band3_AT-1 simulations. The variation in the position of helices 13, 14 and H6 and the change in the position of helix 5 are shown in B. The gate domain of the crystal structure is shown in yellow. C. Position of the K539 and K851 in the mdAE1 crystal structure and at the end of one of our simulations.

<https://doi.org/10.1371/journal.pcbi.1006284.g004>

however in the majority of the simulation it is closer to K539, the H₂DIDS reactive lysine. In particular, the minimum distance between K539 and K851 in the crystal structure is ~1.5 nm while at the end of the atomistic simulation (Band3_AT-1 system) the same distance is reduced to 0.77 ± 0.23 nm (Fig 4C). The C α distance between the same residues in the crystal structure is ~1.9 nm. In our simulations, the K539 C α /K851 C α distance varies between ~1 nm to ~1.5 nm because of the variation in the position of helices 13 and 14 discussed above.

The crystal structure of the mdAE1 dimer revealed a rather loose packing of the two monomers. Using the trj_cavity program [60] we have estimated that the cavity between the two mdAE1 monomers is 7228 Å³. Analysis of the lipid distribution in all our AT simulation suggests that the space between the two dimers in the crystal structure was filled with cholesterol and with the lipid tails of the other phospholipids, mainly the POPS lipids in the inner leaflet (Fig 5). This suggests that cholesterol and other lipids can regulate the interaction between the Band 3 monomers. A POPS lipid can be seen in the simulation without any cholesterol in the bilayer; this lipid was also in the interface in the coarse-grained simulations (Fig 5C). The rest of the space in this case is filled with other lipid tails. The head group of the POPS lipid interacted mainly with lysines and arginines at the cytoplasmic end of helix 5. In the simulations with 50% of cholesterol the space between the two monomers is filled mainly with cholesterol molecules and a single POPS lipid (Fig 5). Interestingly, calculation of the interactions between the two monomers during the atomistic simulations showed that the interactions that were observed in the crystal structure were mostly retained (S4 Fig). In the simulations, additional interactions between residues in region L573 to S595 in the two monomers that are not observed in the crystal structure occurred, allowing the dimer to somewhat optimize its packing. These interactions were higher in the simulations without any cholesterol in the bilayer (S4 Fig). At the end of the simulations with 50% cholesterol the volume of the cavity between the mdAE1 monomers was estimated to 7874 ± 815 Å³. This is close to the volume of the crystal structure (7228 Å³) suggesting that the presence of cholesterol retained the cavity between the two monomers. In contrast, the volume of the cavity in the simulations without any cholesterol in the bilayer was 5595 ± 675 Å³ suggesting that whilst there is still a cavity between the monomers (because of the presence of the lipid tails) this is smaller compared to the crystal structure.

GpA/Band 3 interactions

As mentioned above, Band 3 interacts directly with GPA and this interaction is very important for the trafficking of Band 3 to the cell surface. Despite many functional studies, there is limited structural data for the Band 3/GPA complex. This is partly due to the weak nature of this interaction that makes it challenging to obtain structural information for the nature and dynamics of this complex. To study this complex, we have added the dimeric (residues Arg61-Lys101) transmembrane helical region of the GPA [61,62], and two mdAE1 dimers in a complex bilayer that resembles the native red blood cell plasma membrane (Fig 6A). The structure of GPA [61] revealed a dimeric structure held together by TM helix-helix interactions. Furthermore, it has been shown that Arg61 located in the extracellular unstructured region of GPA interacts directly with Glu658 at the loop connecting TM7 and TM8 of Band 3 to form the Wright blood group antigen [56]. The TM helical part of GPA in our simulations extends

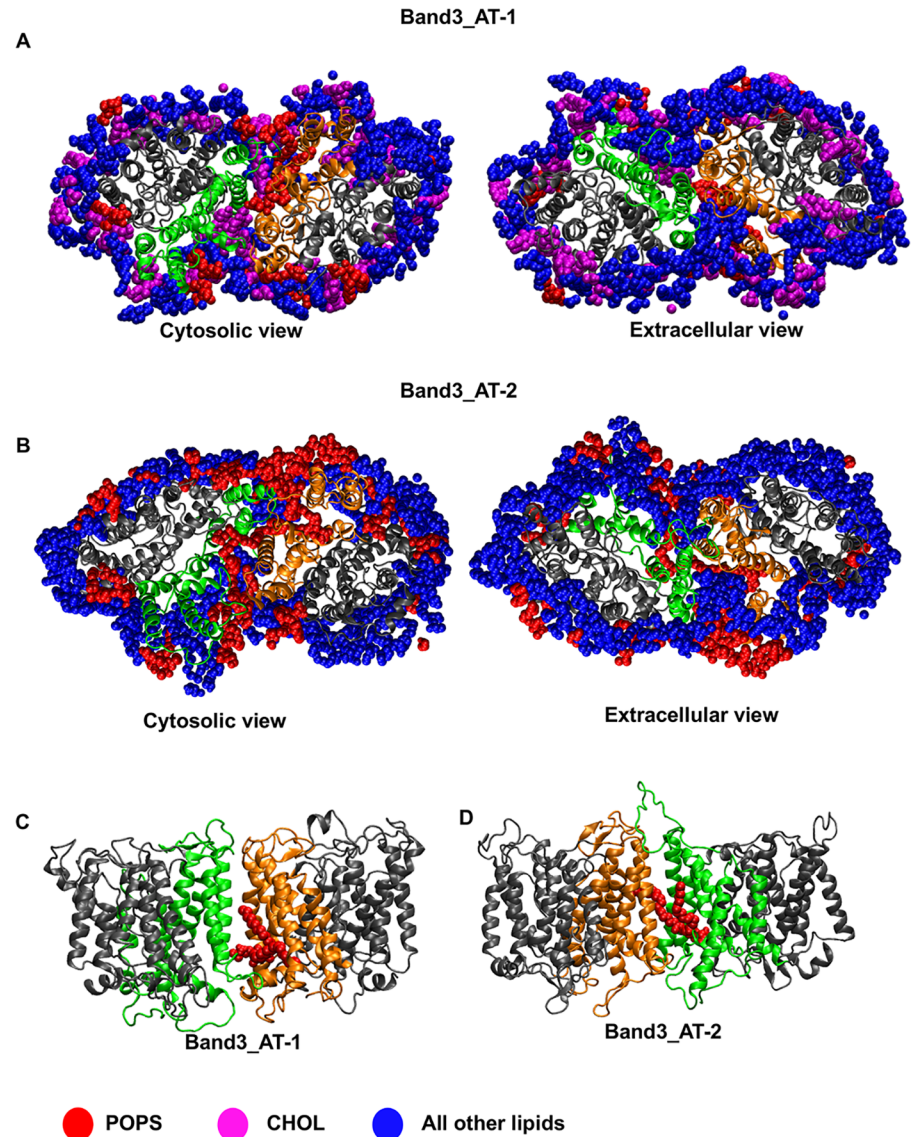


Fig 5. Lipids in the Band 3 dimer interface. A, B. Lipids around the mdAE1 dimer at the end of one of the Band3_AT-1 (A) and Band3_AT-2 (B) simulations. Cholesterol is shown in magenta, POPS in red and the rest of the lipids are shown in blue. C, D. The POPS lipid found between the two monomers of mdAE1 in our simulation is shown for the Band3_AT-1 (C) and Band3_AT-2 (D) simulations. Note that in this Figure we show only the lipids that are in immediate vicinity of the protein. See also S3 Fig.

<https://doi.org/10.1371/journal.pcbi.1006284.g005>

from Ile73 to Arg96. The mdAE1/GPA/mdAE1 complex was modelled so that GPA is at the greatest distance from mdAE1 possible with this ionic interaction restrained during the simulation (see Fig 6A). We have performed 5 simulations of 5 μ s each with one GPA dimer and two mdAE1 dimers (Table 2). Interestingly, in our simulations the transmembrane segments of the GPA dimer interact with the two mdAE1 dimers, forming a bridge between the two Band 3 dimers (Fig 6A). Analysis of the interactions between GPA and mdAE1 in all simulations revealed that GPA interacts with some residues in the following regions of mdAE1: i) Thr481 to Leu484 (top of TM helix 3 and loop connecting TM helices 3 and 4), ii) Val488 to Phe511 (TM helix 4 and the beginning of parallel helix H2), and iii) Trp648 to Phe665 (region connecting TM helices 7 and 8 and top of helix 8). In some of the simulations the GPA also

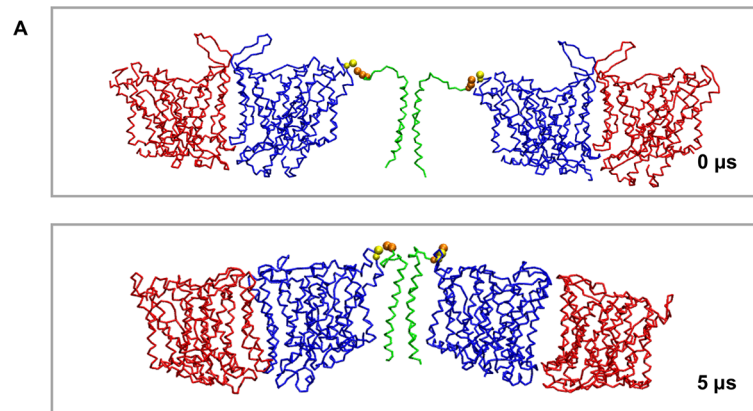


Fig 6. Interactions of Band 3 with GPA. A. Position of the Band 3 dimers and of the GPA dimer at the beginning and at the end of one of the simulations with the Band 3 and GpA dimers. The Band 3 monomers are shown in red and blue and the GPA in green. The GPA Arg61 and Band 3 Glu658 residues that were restrained to interact in one of our simulation systems are shown in yellow and orange VDW, respectively. See also S5, S6, S7, S8 and S9 Figs.

<https://doi.org/10.1371/journal.pcbi.1006284.g006>

interacts with mdAE1 residues Gly381 to Arg384 at the beginning of the parallel helix H1 or with Ala666 to Leu672 residues (TM helix 8; Fig 6 and S5 and S8 Figs). As shown in S8A Fig GPA interacts with Band 3 with residues that face away from the GPA interface. Alignment of the mdAE1/GPA complexes (10 complexes) at the end of the Band3/GPA-1 simulation system suggests that while the GPA TM region interacts with the regions described above it can adopt somewhat modified positions/orientations in some of the simulations.

When the same simulations were performed but without the restraints on the mdAE1 Glu658/ GPA Arg61 interaction, in all simulations GPA interacted in a similar fashion as above but with only one of the mdAE1 dimers (S5C, S5D and S8 Figs). The second mdAE1 dimer diffused away in the bilayer (S6 Fig). This is perhaps expected at this timescale because even in the simulation in which the mdAE1 Glu658-GpA Arg61 interaction was restrained, GPA always interacted first with one of the mdAE1 dimers and after some time it interacted with the other one (S6A Fig). In the simulations where the mdAE1 Glu658-GpA Arg61 interaction is not restrained, GPA Arg61 interactions with Band 3 are rather dynamic. For most of the time, GPA Arg61 interacts with mdAE1 Glu658 but occasionally it interacts with other residues close to 658 or it does not interact with Band 3 at all (S6C and S6D Fig).

To examine how breaking the mdAE1 Glu658/GpA Arg61 interaction would affect the mdAE1/GPA complex formation we have mutated the Glu658 to Lys. This mutation will reverse the charge of residue 658 and will also mimic the Glu658Lys Wright blood group antigen variant. In these simulations, the interaction between Band 3 Lys658/ GpA Arg61 is no longer retained (S7 Fig). However, the helical TM portion and some of the extracellular part of GPA still interacts with the Band 3 TM region in a similar fashion to the simulations above

Table 2. Summary of simulations with Band 3 and GPA.

Simulation	Proteins	Duration
<i>Band3/GpA-1</i>	mdAE1/GPA with Glu658-Arg61 restrained	5 x 5 μs
<i>Band3/GpA-2</i>	mdAE1/GPA with no Glu658-Arg61 restrains	5 x 5 μs
<i>Band3/GpA-3</i>	mdAE1 Glu658Lys/GPA	5 x 5 μs
<i>Band3-large</i>	mdAE1	1 x 10 μs
<i>Band3/GpA-large</i>	mdAE1/GPA complex	1 x 10 μs

<https://doi.org/10.1371/journal.pcbi.1006284.t002>

with the wild type Band 3 (S7 Fig). The Glu658Lys mutation increases the dynamics of the GPA extracellular unstructured region comprised of residues 61 to 65 but the Band3/GPA TM complex can be formed due to the interactions of the GPA helical portion and of residues 66 to 73 that are adjacent to the GPA helical portion with Band 3. In the presence of the Glu658Lys mutation, GPA residues H66, H67, and F68 form the main interactions with Band 3 in the extracellular unstructured part of GPA. Thus, the Wright blood group antigen is probably due to a local conformational change in the epitope rather than complete dissociation of the GPA/Band 3 complex.

Calculation of the interactions of lipids with the GPA-mdAE1 complex reveals the same pattern of interactions as seen above for mdAE1 alone (S9A and S9B Fig). Additional interactions between the cluster of basic residues (Arg96, Arg97, Lys100 and Lys101) on the cytosolic site of GpA and PIP₂ lipids were observed (S9C Fig). Cholesterol is still found in the interface of the two mdAE1 monomers in both dimers of the mdAE1-GPA-mdAE1 complex. Interactions between the cholesterol head group and GpA residues Ser92, Tyr93 and Arg96 to Ile99 in the cytosolic region are also observed (S9 Fig). Preferential interactions of GPA with cholesterol were also shown in other simulation studies [63]. Interestingly, in all systems the cavity in the dimer interface of both mdAE1 was empty at the beginning of our simulations (not occupied by lipids before the equilibration step). In the two systems that contained WT Band 3 (i.e. Band3/GpA-1 and Band3/GpA-2 systems), at the end of the simulations (after equilibration and 5 μ s of simulation) the region in the dimer interface of one of the mdAE1 is occupied by a POPC lipid and cholesterol. The same region of the second mdAE1 is occupied only by cholesterol. In the systems with the mutated mdAE1, in addition to cholesterol one POPC was found in the interface of one of the mdAE1 dimers and three POPC lipids in the interface of the second dimer. This augments our previous observation that the region between the dimer is filled with lipids and cholesterol.

Large-scale simulations of Band 3 and of Band3/GPA complex

Collectively our results above suggest that GPA may promote the clustering of Band 3 dimers. Given that in the Band 3 dimer the two gate domains interact with each other to form the dimer it is possible that a homodimer like GPA may mediate the interactions between the core domains of Band 3 dimers. To test further our observations above we have constructed two large-scale coarse-grained systems with the 64 Band 3 dimers alone or 64 Band 3/GPA complexes inserted in a POPC bilayer (S10A and S10B Fig). We note that in the Band 3/GPA simulation the complex was restrained with an elastic network and therefore no changes in the relative orientation/interactions between Band 3 and GpA were possible. For these simulations we have used the most frequent observed Band 3/GPA complex. In these simulations, the proteins cover ~20% of the surface area to mimic the physiological concentration of Band 3 in red blood cell membranes. We have simulated these two systems for 10 μ s. At the end of the simulation with Band 3 alone, the largest cluster contained 5 dimers but approximately ~45% of the Band 3 dimers in this simulation were not part of a cluster (monomeric) and further ~25% of the Band 3 dimers were part of a cluster with two mdAE1 dimers (dimeric; Fig 7 and S10 Fig). In these simulations, Band 3 dimers interact mainly via residues in regions 478 to 484 in the extracellular loop connecting TM3 and 4, 492 to 507 in TM4, 658 to 670 in TM8 and 857 to 877 in TM14. In contrast, at the end of the simulation with the Band 3/GPA complexes the largest cluster consisted of 8 proteins (during the simulation the largest cluster consisted of 11 proteins) but in this case only ~20% of the Band 3/GPA complexes are not part of a cluster (compared to ~45% in the simulations with Band 3 alone; S10 Fig). Additionally, in the simulation with the Band 3/GPA complexes ~45% of the proteins were part of a cluster that had 5 or

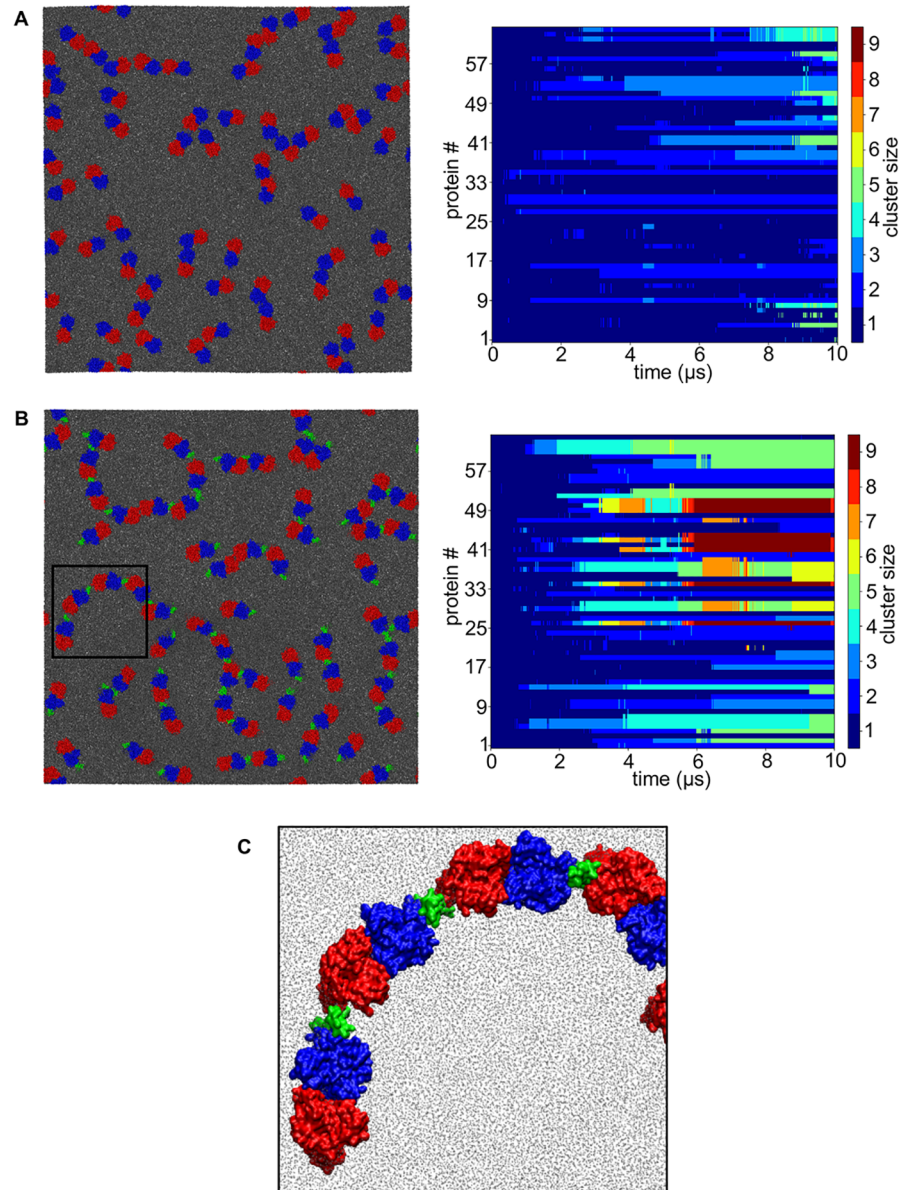


Fig 7. GPA promotes Band 3 clustering. A,B. Final snapshot of the simulations with the mdAE1 dimer and mdAE1/GPA complexes. The mdAE1 monomers are shown in red and blue and the GPA in green. Next to each simulation snapshot we show the clustering of proteins during the simulation as a function of time. Each line represents one protein in our simulation system and each color shows the association of each protein with a specific cluster. C. Zoom-in a region of the simulation in B showing the alternating arrangement of the mdAE1/GpA complex. See also [S10 Fig](#).

<https://doi.org/10.1371/journal.pcbi.1006284.g007>

more proteins. In this simulation, the interaction between Band 3 dimers is mediated in most cases via the GPA as predicted in our simulations above and most of the time Band 3 and GPA are in a linear arrangement in good agreement with our simulations above (Fig 7). We also note that in the simulations with the Band 3/GPA complexes, clusters with four proteins or more were formed after approximately 2 μ s of simulation whereas in the simulation with the Band 3 alone similar clusters (with 4 proteins or more) were formed after approximately 7.5 μ s of simulation. Calculation of the anomalous diffusion of the two simulation systems showed that in the Band 3 simulation the diffusion coefficient was $4.08 \pm 0.32 \times 10^{-7} \text{ cm}^2/\text{s}$ (scaling

exponent of the non-linear fit value was 0.85 ± 0.01) whereas the diffusion coefficient of the Band 3/GPA complex was $3.24 \pm 0.25 \times 10^{-7} \text{ cm}^2/\text{s}$ (scaling exponent of the non-linear fit value was 0.84 ± 0.01). Collectively, our results suggest that the presence of GPA promoted the clustering of Band 3 in red blood cell membranes.

Discussion

In this study, we have created the first realistic atomistic model of mdAE1 in a complex lipid bilayer that mimics the native red cell membrane. Our MD simulations have shown preferential interaction of acidic lipids (POPS and PIP₂) on the inner leaflet of the bilayer with specific sites on mdAE1. POPS has been shown to destabilize AE1 [42] and reduce its transport activity [39]. Thus, this acidic lipid may play a role in regulating the transport activity of Band 3 by binding to particular sites in the protein.

Phosphatidylinositol-4-phosphate kinase is associated with the human red cell membrane [64] and its product, PIP₂ is involved in modulating Protein 4.1 interactions with erythrocyte membrane proteins, inhibiting binding to Band 3 and enhancing binding to Glycophorin C [65,66]. We found that PIP₂ binds preferentially to specific sites on mdAE1. The high content of Band 3 in the erythrocyte membrane would sequester the bulk of this lipid to an annulus around Band 3 providing a “hot spot” for protein interactions and signaling.

We found that cholesterol interacts directly with the surface of mdAE1, an interaction that involves specific tryptophan residues. The human β 2-adrenergic receptor was co-crystallized with a tightly-bound cholesterol molecule involving a close interaction with a tryptophan residue that stabilizes the protein [67,68]. Cholesterol binding sites were also identified at the mdAE1 dimer interface, suggesting that cholesterol may play a role in stabilizing or modulating the interaction between mdAE1 subunits. A number of biophysical studies have supported the view that cholesterol interacts with Band 3 and affects its dynamics, self-association and transport activity. It has been shown that cholesterol affects the aggregation state of Band 3 [69]. Band 3 has a high-affinity inhibitory cholesterol binding site [44]. A strong interaction of spin-labelled cholesterol with Band 3 has also been demonstrated [45]. Enriching cholesterol in red blood cells inhibits transport, while depleting cholesterol enhances transport [49]. Thus, cholesterol interaction with Band 3 modulates its transport activity, likely by rigidifying the dimer interface.

It has been suggested that cholesterol interacts at distinct binding sites in membrane proteins that consist of CRAC, CARC or tilted domains containing tyrosine residues [70]. The CRAC domain has a signature sequence L/V-X1-5-Y-X1-5-K/R while the CARC has the opposite orientation. MdAE1 in our simulations contains 14 tyrosine residues, of which 12 have basic residues +/- 5 residues away. Note, however, that Tyr 390/392/393, and Tyr 553/555 are very close to each other. The basic residue interacts with the hydroxyl group, the tyrosine with the cholesterol rings, and the Leu/Ile/Val with the isoocetyl chain. TM5 contains the “CRAC” sequence-**ISLIFIY⁵³⁴ETFSK**- at its C-terminal end. The isoleucine and tyrosine are on the same side of TM helix 5 facing the bilayer, however Lys539 is the H₂DIDS reactive lysine facing the inhibitor-binding site. Interestingly in our coarse-grained simulation we observe the highest number of interaction with cholesterol close to Tyr 390, Tyr 413 and Tyr 534.

Band 3 exists in three populations in human erythrocytes: 1) tetrameric Band 3 associates with GPA, Ankyrin, protein 4.2 and the Rh complex in the Ankyrin-associated complex, 2) the junctional complex of spectrin, actin and protein 4.1, and 3) a freely mobile dimer fraction [71]. There is also considerable evidence that Band 3 and GPA interact in the red cell membrane [72]. The Wright blood group antigen involves the direct interaction of Arg61 on the extracellular part of GPA with Glu658 in the extracellular loop connecting TM7 and TM8 in

Band 3 [56] and anti Wra antibodies can co-immunoprecipitate GPA and Band 3 [73]. In Band 3 knockout mice, GPA is absent [74]. Biophysical evidence [75–77] suggest that GPA is associated with Band 3 in the red cell membrane as anti-GPA antibodies have been shown to decrease the rotational mobility of Band 3. A recent study [78] of the diffusion of GPA in human erythrocytes using quantum dots, however, showed that perturbation of Band 3 diffusion does not affect GPA diffusion. Our studies show that GPA can interact directly with Band 3 outside of the Ankyrin complex.

The interaction of GPA with Band 3 has two distinct physiological consequences: 1) enhanced trafficking of Band 3 from the ER to the plasma membrane, and 2) stimulation of anion transport activity [50,51]. Studies using GPA/GPB chimeras and point mutations [79] have shown that extracellular portions of GPA proximal to Arg61 that interacts with Glu658 to form the Wr antigen stimulate transport. In our simulations, we also observe interaction of residues on GPA that are proximal to Arg61 with Band 3. The extracellular interactions of GPA with Band 3 were maintained in the E658K mutant with GPA H66, H67 and F68 forming the main interactions with Band 3. The C-terminal cytoplasmic tail of GPA enhances trafficking via interaction around G701 on the cytosolic end of TM9 in Band 3. Indeed, the trafficking of the dRTA G701D mutant can be rescued by GPA [80]. In our simulations we don't see any significant interactions of GPA with G701 but this may be due to the fact that we use a GPA with a very short cytosolic region. Furthermore, GPA mutations that interfere with dimer formation are still able to enhance Band 3 trafficking [53].

In the simulations of 64 mdAE1 dimers and 64 GPA dimers we found that GPA could bridge mdAE1 dimers forming dynamic strands of alternating GPA dimers and mdAE1 dimers. This clustering may play a key role in accumulating these two proteins at the exit sites in the ER membrane where COPII vesicles bud off to traffic newly synthesized proteins to the Golgi [81]. This may account for the stimulatory effect that GPA has on Band 3 trafficking to the cell surface. It is noteworthy that GPA can rescue the trafficking of the Southeast Asian Ovalocytosis (SAO) Band 3 deletion mutant to the cell surface [52]. This indicates that the GPA interaction with this misfolded form of Band 3 is maintained. It has been shown recently that the SAO deletion mutation changes the dynamics of the first TM helix of Band 3 in a lipid bilayer and also removes the proline induced bend [82]. In the future, we plan to use MD simulations to study the effect of the SAO deletion on Band 3 folding and its interaction with GPA.

Limitations

It is important to consider possible limitations of the simulations used in the study. We have used the dimeric TM region of mdAE1 that was in the outward open conformation. The cytosolic domain of mdAE1 is not present in our simulation, however, it may affect the behavior of mdAE1 e.g. it is known that the cytosolic domain interacts with the cytoskeleton. We note that whilst there are crystal structures of the separate mdAE1 and cdAE1, a complete Band 3 structure is not yet available. Therefore, there is still some uncertainty about the orientation of the cytosolic domain relative to the TM region of mdAE1. For this reason, in this study we have focused on the TM region of mdAE1 but as more structural data about the complete mdAE1 become available it would be interesting to examine how the presence of the cytosolic domain of Band 3 affects the ability of Band 3 to form tetramers and its interaction with lipids and GPA.

The use of a coarse-grained model implies some approximations on the protein and the lipids. In our CG-MD simulations we have used an elastic network model. This model restrained the protein in an outward conformation. Atomistic simulations using the last snapshot of the CG-MD systems partly address this limitation, but more extended simulations or enhanced sampling techniques will be needed to address the conformational dynamics of mdAE1. Such

simulation may also demonstrate how conformational changes within the protein (e.g. from outward to inward-facing state) can change its interaction with lipids. Regarding the mdAE1 interaction with GPA, we observe only the formation of the mdAE1-GPA complex, not its dissociation. This may be partly due to the timescale of the simulations. It has also been recently suggested that CG-MD simulations may exaggerate protein-protein interactions [83]. Whilst it has been suggested that the mdAE1-GPA interaction is likely to be weak, our current simulations do not allow us to give an estimate on the strength of the interactions between mdAE1 and GPA. They do provide, however, a molecular model that explains in detail the mdAE1-GPA interaction. To estimate the affinity of GPA to mdAE1 one could perform free energy calculations [84–86] although further developments of this methodology may be required to be applicable to larger protein-protein complexes such as the mdAE1/GPA complex.

Material and methods

Coarse-grained molecular dynamics (CG-MD) simulations

The CG-MD simulations were performed using the Martini 2.2 force field [87,88] and GRO-MACS [89]. For the CG-MD simulations the crystal structure of Band 3 dimer (PDB: 4YZF [11]) was converted to a coarse-grained resolution. An elastic network using a cut-off distance of 7 Å to model the protein secondary and tertiary structure was used. The elastic network restricts any major conformational change within the protein during the CG-MD simulations. We also note that prior to the conversion to the coarse-grained representation, the H₂DIDS substrate that was included in the crystal structure was removed. Additionally, the missing unstructured regions from the crystal structure were added using Modeller [90,91].

A POPC bilayer was then self-assembled around the mdAE1 dimer (see [1]). The last snapshot from the aforementioned simulation was taken and 8 different systems were generated (see Table 1) with the protein inserted in complex asymmetric bilayers that resemble properties of the *in vivo* red blood cell plasma membrane. The exchange of lipids was done as described in [57]. All simulation systems were solvated with CG water particles and ~150 nM of NaCl was added to neutralize the systems. Prior to the production simulation all systems that did not contained SM were equilibrated for 2 ns with the protein backbone particles restrained. Systems with SM in the bilayer were equilibrated for 5 ns. Note that we have performed five self-assembly simulations and in all simulations the mdAE1 dimer interface region was occupied by lipids. In three of the simulations one lipid occupied the dimer interface during the simulations. In the other simulations two or three lipids were in the dimer interface. For that reason, for the exchange of lipids we have used one of the three systems in which a lipid was embedded in the dimer interface.

For the simulation of the mdAE1/GpA/mdAE1 complex the protein was inserted in a pre-formed POPC bilayer. Subsequently, two systems were generated with the protein inserted in complex asymmetric bilayers that resemble properties of the *in vivo* red blood cell plasma membrane. In one of the systems an additional restrain was added between GPA Arg61 and mdAE1 Glu658 residues. Prior to the production simulation the Band3/GpA-1 and Band3/GpA-2 systems were equilibrated for 40 ns and the Band3/GpA-3 for 90 ns with the protein backbone particles restrained (see Table 2).

To generate the large-scale systems a POPC bilayer was self-assembled around the mdAE1 dimer or the mdAE1/GPA complex. Then, the system with one protein was replicated in the xy plane using the GROMACS command genconf to create a system with 64 mdAE1 and or 64 mdAE1/GPA proteins.

The temperature for the CG-MD simulation was set to 323 K. The V-rescale thermostat [92] (coupling constant of 1.0) was used for temperature control. A Parrinello-Rahman

barostat [93] (a coupling constant of 1.0 and a reference pressure of 1 bar) was used for pressure control. The integration step was 20 fs for the simulations with the Band 3 and the large-scale simulations and 10 fs for the simulations with the mdAE1/GpA/mdAE1 complex. Lennard-Jones and Coulombic interactions were shifted to zero between 9 and 12 Å, and between 0 and 12 Å, respectively.

Atomistic molecular dynamics simulations (AT-MD)

The final snapshots of 3 repeat simulations from Band3-1 and Band3-7 simulation systems were converted to atomistic resolution as described in Stansfeld *et al.* [59]. Atomistic simulations were run using the GROMOS53a6 force field. The simulations were run for 250 ns. The V-rescale thermostat [92] and the Parrinello-Rahman barostat [93] were used for temperature and pressure control, respectively. The Particle Mesh Ewald (PME) was used to model long-range electrostatic interactions [94]. The LINCS algorithm was used to constrain bond lengths [95]. Prior to the production simulations the systems were equilibrated with the protein C α atoms restrained for 2 ns. The simulation timestep was 2 fs and the temperature was set to 323 K. A similar approach has been used previously to study the interaction of e.g. aquaporin/PE [96], for Kir/PIP₂ [97] and ANT/CL [98] and it yields good agreement with experimental data.

Diffusion analysis

The diffusion analysis was performed using the open source code: <https://zenodo.org/record/11827#.Whvg2racZ-U>. For this analysis, the last 7 μ s and 5 μ s were used for the simulation with one Band 3 in the bilayer and the large-scale simulations, respectively. For all systems, the lateral diffusion was calculated. The errors for the diffusion coefficient of the systems in Table 1 is the standard deviation of the diffusion coefficient between the five replicas. The errors for the diffusion coefficient of the large-scale systems were calculated by the aforementioned code.

Clustering analysis

Clustering analysis of the proteins was performed using the open source code: https://github.com/jhelie/cluster_prot.

CG2AT

Simulation systems were converted to atomistic resolution as described in Stansfeld *et al.* [59].

Analysis of the Band 3 dimer interface cavity

The calculation of the volume of the cavity in the interface of the Band 3 dimer was done using `trj_cavity` (<https://sourceforge.net/projects/trjcavity/>) [60]. Note that for this calculation we have used a `ndx` file that consisted the helices that form the Band 3 dimer interface. The calculation was done using either the Band 3 crystal structure or the last snapshot of the atomistic simulations. The errors for the volume of the cavity is the standard deviation of the volumes between the three replicas.

Supporting information

S1 Fig. A. Normalized contacts between mdAE1 and PIP₂ (A), POPS (B), POPE (C), and cholesterol (D) head groups. For these histograms, the normalized contacts between the aforementioned lipids and mdAE1 from the different coarse-grained simulation systems that contained the lipids were added together. All 8 systems contained POPS and POPE lipids, 7

systems contained cholesterol and 2 systems contained PIP₂ molecules.
(TIF)

S2 Fig. A. Normalized contacts between mdAE1 and POPS and PIP₂ molecules from the Band3-7 system. For the normalization, the number of contacts of each residue was divided by the total number of frames and the number of lipids in each simulation. This analysis demonstrates the preference of Band 3 to interact with PIP₂ molecules. B. Convergence analysis of the interactions of mdAE1 with the lipids. The spatial distribution of PIP₂ and cholesterol around mdAE1 in the Band3-7 system is shown for 1, 3, and 5 repeat simulations.
(TIF)

S3 Fig. A. Normalized contacts between mdAE1 and PIP₂ or cholesterol head groups (A) from the Band3_AT-1 atomistic simulations. For this analysis, the contacts from the 3 independent atomistic simulations were added together.
(TIF)

S4 Fig. A, B. Contacts between the two mdAE1 monomers in our atomistic simulations (calculated for the last 30 ns of the atomistic simulations). The contacts for one of the mdAE1 proteins are shown in red and for the other proteins are shown in blue. The green vertical lines indicate the contacts found in the Band 3 crystal structure. A cut off distance of 0.4 nm was used to define a contact. The contacts are the average of 3 repeat atomistic simulations.
(TIF)

S5 Fig. A, B, C, D. Normalized contacts between mdAE1 and GPA in our coarse-grained simulations with the two mdAE1 dimers and GPA. The contacts are shown for the simulation system in which we restrained the GPA Arg61/Band 3 Glu658 interaction (A, B) and for the simulation system without any restrains in the GPA Arg61/Band 3 Glu658 interaction (C, D). Because in C and D GPA interacts with only one of the monomers, the interactions from all Band 3/GPA complexes were added together.
(TIF)

S6 Fig. A, B. Minimum distance between mdAE1 dimers and the transmembrane region of GPA for the simulations in which we restrained the GPA Arg61/Band 3 Glu658 interaction (A) and for the simulations without any restrains in the GPA Arg61/Band 3 Glu658 interaction (B). Note that in the simulations in which we did not include restrains in the GPA Arg61/Band 3 Glu658 interaction one of dimers diffuses away. C. Normalized contacts between mdAE1 and GPA Arg61 in the simulations without any restrains in the GPA Arg61/mdAE1 Glu658 interaction. The contacts from all systems were added together for this analysis. D. Minimum distance between mdAE1 and GPA Arg61 (black) or mdAE1 Glu658 and GPA Arg61 (red) is shown from one of the simulations.
(TIF)

S7 Fig. A, B. Minimum distance between mdAE1 and GPA (A) and mdAE1 residue Lys658 and GPA residue Arg61 (B) is shown from one of the Band3/GpA-3 simulations. C. Normalized contacts between mdAE1 and GPA in our simulations with the GPA Arg61/Band 3 Glu658Lys mutation. Note that the interactions from all Band 3/GPA complexes were added together.
(TIF)

S8 Fig. A. Final snapshots of the 5 repeat simulations of the Band3/GpA-1 system demonstrating the arrangement of the Band3/GPA/Band3 complex. The Band 3 monomers are shown in red and blue and the GPA in green. B. Alignment of the Band 3/GPA complexes from the

Band3/GpA-1 system. The 10 different complexes are shown in different color. The four different positions of the GPA when bound on Band 3 are shown separately. C. Alignment of the Band 3/GPA complexes from the Band3/GpA-2 and Band3/GpA-3 systems. The 5 different complexes are shown in different color. Note that for clarity in B and C we show only the helical region of the GPA helix that interacts with Band 3.

(TIF)

S9 Fig. A, B, C, D. Normalized contacts between mdAE1 (A, B) or GPA (C, D) and PIP₂ or cholesterol head groups from the Band3/GpA-1 simulation. For this analysis, the contacts from the 5 independent simulations were added together. For the normalization, the number of contacts of each residue was divided by the total number of frames and the number of lipids in each simulation.

(TIF)

S10 Fig. Snapshot from the start of the Band3-large (A) and Band3/GPA-large (B) simulations. The mdAE1 monomers are shown in red and blue and the GPA in green. C, D. Protein-protein interaction in A and B. The contacts are mapped onto the structure of the Band 3 dimer (for A) and of the Band 3/GPA complex (for B). Blue represents no/low number of contacts, white represents medium number of contacts and red high number of contacts. For this analysis, the contacts for all 64 individual proteins complexes in each system were added together. The contacts were calculated for the last 1 μ s of the simulation to allow formation of the protein clusters. E, F. Clustering dynamics shown as the percentage of Band 3 (E) or Band 3/GPA (F) cluster size as a function of the simulation time.

(TIF)

Acknowledgments

This project was initiated during a sabbatical leave of RAFR in the laboratory of Prof. Mark Sansom at the University of Oxford.

Author Contributions

Conceptualization: Antreas C. Kalli, Reinhart A. F. Reithmeier.

Data curation: Antreas C. Kalli.

Formal analysis: Antreas C. Kalli.

Funding acquisition: Antreas C. Kalli.

Investigation: Antreas C. Kalli.

Methodology: Antreas C. Kalli.

Project administration: Antreas C. Kalli, Reinhart A. F. Reithmeier.

Resources: Antreas C. Kalli, Reinhart A. F. Reithmeier.

Software: Antreas C. Kalli.

Supervision: Reinhart A. F. Reithmeier.

Validation: Antreas C. Kalli.

Visualization: Antreas C. Kalli.

Writing – original draft: Antreas C. Kalli, Reinhart A. F. Reithmeier.

Writing – review & editing: Antreas C. Kalli, Reinhart A. F. Reithmeier.

References

1. Reithmeier RAF, Casey JR, Kalli AC, Sansom MSP, Alguel Y, Iwata S. Band 3, the human red cell chloride/bicarbonate anion exchanger (AE1, SLC4A1), in a structural context. *Biochim Biophys Acta—Bio-membr.* 2016; 1858: 1507–1532. <https://doi.org/10.1016/j.bbamem.2016.03.030> PMID: 27058983
2. Low PS. Structure and function of the cytoplasmic domain of Band 3: Centre of erythrocyte membrane-peripheral protein interactions. *Biochim Biophys Acta.* 1986; 864: 145–167. [http://dx.doi.org/10.1016/0304-4157\(86\)90009-2](http://dx.doi.org/10.1016/0304-4157(86)90009-2) PMID: 2943319
3. Lux SE, John KM, Kopito RR, Lodish HF. Cloning and characterization of band 3, the human erythrocyte anion-exchange protein (AE1). *Proc Natl Acad Sci U S A.* 1989; 86: 9089–9093. <https://doi.org/10.1073/pnas.86.23.9089> PMID: 2594752
4. Tanner MJ, Martin PG, High S. The complete amino acid sequence of the human erythrocyte membrane anion-transport protein deduced from the cDNA sequence. *Biochem J.* 1988; 256: 703–12. Available: <http://www.pubmedcentral.nih.gov/articlerender.fcgi?artid=1135473&tool=pmcentrez&rendertype=abstract> PMID: 3223947
5. Jennings ML. Oligomeric structure and the anion transport function of human erythrocyte band 3 protein. *J Mem Biol.* 1984; 80: 105–117. <https://doi.org/10.1007/BF01868768>
6. Casey JR, Reithmeier RAF. Analysis of the oligomeric state of Band 3, the anion transport protein of the human erythrocyte membrane, by size exclusion high performance liquid chromatography. Oligomeric stability and origin of heterogeneity. *J Biol Chem.* 1991; 266: 15726–15737. Available: <http://www.jbc.org/content/266/24/15726.abstractN2> PMID: 1874731
7. Zhang D, Kiyatkin A, Bolin JT, Low PS. Crystallographic structure and functional interpretation of the cytoplasmic domain of erythrocyte membrane band 3. *Blood.* 2000; 96: 2925–33. Available: <http://www.bloodjournal.org/content/96/9/2925.abstract> PMID: 11049968
8. Reithmeier RA. Fragmentation of the band 3 polypeptide from human erythrocyte membranes. *J Biol Chem.* 1979; 254: 3054–3060. Available: http://www.ncbi.nlm.nih.gov/entrez/query.fcgi?cmd=Retrieve&db=PubMed&dopt=Citation&list_uids=429334 PMID: 429334
9. Wang DN, Kühlbrandt W, Sarabia V, Reithmeier RAF. Two-dimensional structure of the membrane domain of human Band 3, the anion transport protein of erythrocyte membrane. *EMBO J.* 1993; 12: 2233–2239. Available: <http://www.ncbi.nlm.nih.gov/pmc/articles/PMC413451/> PMID: 8508760
10. Wang DN, Sarabia VE, Reithmeier RA, Kuhlbrandt W. Three-dimensional map of the dimeric membrane domain of the human erythrocyte anion exchanger, Band 3. *EMBO J.* 1994; 13: 3230–3235. Available: <http://www.ncbi.nlm.nih.gov/pubmed/8045253> PMID: 8045253
11. Arakawa T, Kobayashi-Yurugi T, Alguel Y, Iwanari H, Hatae H, Iwata M, et al. Crystal structure of the anion exchanger domain of human erythrocyte band 3. *Science (80-).* 2015; 350: 680–684. <https://doi.org/10.1126/science.aaa4335> PMID: 26542571
12. Tang XB, Fujinaga J, Kopito R, Casey JR. Topology of the region surrounding Glu681 of human AE1 protein, the erythrocyte anion exchanger. *J Biol Chem.* 1998; 273: 22545–22553. <https://doi.org/10.1074/jbc.273.35.22545> PMID: 9712881
13. Zhu Q, Lee DWK, Casey JR. Novel topology in C-terminal region of the human plasma membrane anion exchanger, AE1. *J Biol Chem.* 2003; 278: 3112–3120. <https://doi.org/10.1074/jbc.M207797200> PMID: 12446737
14. Fujinaga J, Tang XB, Casey JR. Topology of the membrane domain of human erythrocyte anion exchange protein, AE1. *J Biol Chem.* 1999; 274: 6626–33. <https://doi.org/10.1074/jbc.274.10.6626> PMID: 10037758
15. Popov M, Tam LY, Li J, Reithmeier RAF. Mapping the ends of transmembrane segments in a polytopic membrane protein. *J Biol Chem.* 1997; 272: 18325–18332. <https://doi.org/10.1074/jbc.272.29.18325> PMID: 9218473
16. Popov M, Li J, Reithmeier RA. Transmembrane folding of the human erythrocyte anion exchanger (AE1, Band 3) determined by scanning and insertional N-glycosylation mutagenesis. *Biochem J.* 1999; 339: 269–79. <https://doi.org/10.1042/0264-6021:3390269> PMID: 10191257
17. Hamasaki N, Okubo K, Kuma H, Kang D, Yae Y. Proteolytic cleavage sites of band 3 protein in alkali-treated membranes: fidelity of hydropathy prediction for band 3 protein. *J Biochem.* 1997; 122: 577–585. Available: <papers2://publication/uuid/523B8B76-B70E-46A8-B307-DF0C06F463A5> PMID: 9348087
18. Reyes G, Nivillac NMI, Chalsev M, Coe IR. Analysis of recombinant tagged equilibrative nucleoside transporter 1 (ENT1) expressed in *E. coli*. *Biochem Cell Biol.* NRC Research Press; 2011; 89: 246–255. <https://doi.org/10.1139/o10-155> PMID: 21455275
19. Groves JD, Tanner MJ. Structural model for the organization of the transmembrane spans of the human red-cell anion exchanger (band 3; AE1). *Biochem J.* 1999; 344 Pt 3: 699–711. <https://doi.org/10.1042/0264-6021:3440699>

20. Barneaud-Rocca D, Etchebest C, Guizouarn H. Structural model of the anion exchanger 1 (SLC4A1) and identification of transmembrane segments forming the transport site. *J Biol Chem.* 2013; 288: 26372–26384. <https://doi.org/10.1074/jbc.M113.465989> PMID: 23846695
21. Lu F, Li S, Jiang Y, Jiang J, Fan H, Lu G, et al. Structure and mechanism of the uracil transporter UraA. *Nature.* Nature Publishing Group, a division of Macmillan Publishers Limited. All Rights Reserved.; 2011; 472: 243–247. <https://doi.org/10.1038/nature09885> PMID: 21423164
22. Geertsma ER, Chang YN, Shaik FR, Neldner Y, Pardon E, Steyaert J, et al. Structure of a prokaryotic fumarate transporter reveals the architecture of the SLC26 family. *Nat Struct Mol Biol.* Nature Publishing Group, a division of Macmillan Publishers Limited. All Rights Reserved.; 2015; 22: 803–808. <https://doi.org/10.1038/nsmb.3091> PMID: 26367249
23. Alguet Y, Amillis S, Leung J, Lambrinidis G, Capaldi S, Scull NJ, et al. Structure of eukaryotic purine/H⁺ symporter UapA suggests a role for homodimerization in transport activity. *NAT Commun.* Nature Publishing Group; 2016; 7: 11336. <https://doi.org/10.1038/ncomms11336> PMID: 27088252
24. Chang YN, Geertsma ER. The novel class of seven transmembrane segment inverted repeat carriers [Internet]. *Biological Chemistry.* 2017. pp. 165–174. <https://doi.org/10.1515/hsz-2016-0254> PMID: 27865089
25. Falke JJ, Chan SI. Evidence that anion transport by band 3 proceeds via a ping-pong mechanism involving a single transport site. A 35Cl NMR study. *J Biol Chem.* 1985; 260: 9537–9544. Available: <http://www.jbc.org/content/260/17/9537.abstractN2> PMID: 4019484
26. Coincon M, Uzdavynys P, Nji E, Dotson DL, Winkelmann I, Abdul-Hussein S, et al. Crystal structures reveal the molecular basis of ion translocation in sodium/proton antiporters. *Nat Struct Mol Biol.* Nature Publishing Group, a division of Macmillan Publishers Limited. All Rights Reserved.; 2016; 23: 248–255. <https://doi.org/10.1038/nsmb.3164> PMID: 26828964
27. Reithmeier RAF, Moraes TF. Solute carriers keep on rockin'. *Nat Struct Mol Biol.* Nature Publishing Group, a division of Macmillan Publishers Limited. All Rights Reserved.; 2015; 22: 752–754. <https://doi.org/10.1038/nsmb.3104> PMID: 26439635
28. Fici E, Faraldo-Gómez JD, Jennings ML, Forrest LR. Asymmetry of inverted-topology repeats in the AE1 anion exchanger suggests an elevator-like mechanism. *J Gen Physiol.* 2017; 149: 1149–1164. <https://doi.org/10.1085/jgp.201711836> PMID: 29167180
29. Cabantchik ZI, Rothstein A. The nature of the membrane sites controlling anion permeability of human red blood cells as determined by studies with disulfonic stilbene derivatives. *J Membr Biol.* 1972; 10: 311–330. <https://doi.org/10.1007/BF01867863> PMID: 4667922
30. Cabantchik ZI, Rothstein A. Membrane proteins related to anion permeability of human red blood cells—Localization of disulfonic stilbene binding sites in proteins involved in permeation. *J Membr Biol.* 1974; 15: 207–226. <https://doi.org/10.1007/BF01870088> PMID: 4838037
31. Okubo K, Kang D, Hamasaki N, Jennings ML. Red blood cell band 3. Lysine 539 and lysine 851 react with the same H2DIDS (4,4'-diisothiocyanodihydrostilbene-2,2'-disulfonic acid) molecule. *J Biol Chem.* 1994; 269: 1918–1926. Available: <http://www.jbc.org/content/269/3/1918.abstractN2> PMID: 8294441
32. Snow JW, Brandts JF, Low PS. The effects of anion transport inhibitors on structural transitions in erythrocyte membranes. *Biochim Biophys Acta.* 1978; 512: 579–591. [http://dx.doi.org/10.1016/0005-2736\(78\)90167-0](http://dx.doi.org/10.1016/0005-2736(78)90167-0) PMID: 708734
33. Maneri LR, Low PS. Structural Stability of the Erythrocyte Anion Transporter, Band 3, in Different Lipid Environments. *J. Biol. Chem.* 1988; 263: 16170–16178. <http://www.jbc.org/content/263/31/16170.long>
34. Davio SR, Low PS. Characterization of the Calorimetric C Transition of the Human Erythrocyte Membrane. *Biochemistry.* Am. Chem. Soc.; 1982; 21: 3585–3593. <https://doi.org/10.1021/bi00258a009>
35. Lange C, Hunte C. Crystal structure of the yeast cytochrome bc1 complex with its bound substrate cytochrome c. *Proc Natl Acad Sci.* 2002; 99: 2800–2805. <https://doi.org/10.1073/pnas.052704699> PMID: 11880631
36. Lemieux MJ, Reithmeier RAF, Wang DN. Importance of detergent and phospholipid in the crystallization of the human erythrocyte anion-exchanger membrane domain. *J Struct Biol.* 2002; 137: 322–332. [https://doi.org/10.1016/S1047-8477\(02\)00010-2](https://doi.org/10.1016/S1047-8477(02)00010-2) PMID: 12096900
37. Newstead S, Ferrandon S, Iwata S. Rationalizing α -helical membrane protein crystallization. *Protein Sci.* Cold Spring Harbor Laboratory Press; 2008; 17: 466–472. <https://doi.org/10.1110/ps.073263108> PMID: 18218713
38. Kalli AC, Sansom MSP, Reithmeier RAF. Molecular Dynamics Simulations of the Bacterial UraA H⁺-Uracil Symporter in Lipid Bilayers Reveal a Closed State and a Selective Interaction with Cardiolipin. *PLoS Comput Biol.* Public Library of Science; 2015; 11: e1004123. <https://doi.org/10.1371/journal.pcbi.1004123> PMID: 25729859

39. Köhne W, Deuticke B, Haest CWM. Phospholipid dependence of the anion transport system of the human erythrocyte membrane. Studies on reconstituted band 3/lipid vesicles. *BBA—Biomembr.* 1983; 730: 139–150. [https://doi.org/10.1016/0005-2736\(83\)90326-7](https://doi.org/10.1016/0005-2736(83)90326-7)
40. Maneri LR, Low PS. Fatty acid composition of lipids which copurify with band 3. *Biochem Biophys Res Commun.* 1989; 159: 1012–1019. [https://doi.org/10.1016/0006-291X\(89\)92209-2](https://doi.org/10.1016/0006-291X(89)92209-2) PMID: 2930548
41. Nigg EA, Cherry RJ. Influence of Temperature and Cholesterol on the Rotational Diffusion of Band 3 in the Human Erythrocyte Membrane. *Biochemistry.* American Chemical Society; 1979; 18: 3457–3465. <https://doi.org/10.1021/bi00583a004> PMID: 224909
42. Maneri LR, Low PS. Structural stability of the erythrocyte anion transporter, band 3, in different lipid environments. A differential scanning calorimetric study. *J Biol Chem.* 1988; 263: 16170–16178. Available: http://www.ncbi.nlm.nih.gov/entrez/query.fcgi?cmd=Retrieve&db=PubMed&dopt=Citation&list_uids=3182790 PMID: 3182790
43. Klugerman AH, Gaarn A, Parkes JG. Effect of cholesterol upon the conformation of band 3 and its transmembrane fragment. *Can J Biochem Cell Biol.* NRC Research Press; 1984; 62: 1033–1040. <https://doi.org/10.1139/o84-132> PMID: 6509361
44. Schubert D, Boss K. Band 3 protein-cholesterol interactions in erythrocyte membranes. Possible role in anion transport and dependency on membrane phospholipid. *FEBS Lett.* 1982; 150: 4–8. [https://doi.org/10.1016/0014-5793\(82\)81295-7](https://doi.org/10.1016/0014-5793(82)81295-7) PMID: 7160474
45. Seigneuret M, Favre E, Morrot G, Devaux PF. Strong interactions between a spin-labeled cholesterol analog and erythrocyte proteins in the human erythrocyte membrane. *BBA—Biomembr.* 1985; 813: 174–182. [https://doi.org/10.1016/0005-2736\(85\)90231-7](https://doi.org/10.1016/0005-2736(85)90231-7)
46. Schubert D, Marie H. The Structure of Mixed Cholesterol-Phospholipid Monolayers Spread at the Air-Water-Interface as Probed by Interactions with Band-3 Protein from Erythrocyte-Membranes. *Biochim Biophys Acta.* 1982; 684: 75–82. [http://dx.doi.org/10.1016/0005-2736\(82\)90051-7](http://dx.doi.org/10.1016/0005-2736(82)90051-7) PMID: 7055556
47. Rodgers W, Glaser M. Distributions of Proteins and Lipids in the Erythrocyte Membrane. *Biochemistry.* American Chemical Society; 1993; 32: 12591–12598. <https://doi.org/10.1021/bi00210a007> PMID: 8251477
48. Pap EHW, Hanicak A, van Hoek A, Wirtz KWA, Visser AJWG. Quantitative Analysis of Lipid-Lipid and Lipid-Protein Interactions in Membranes by Use of Pyrene-Labeled Phosphoinositides. *Biochemistry.* American Chemical Society; 1995; 34: 9118–9125. <https://doi.org/10.1021/bi00028a022> PMID: 7619810
49. Gregg VA, Reithmeier RAF. Effect of cholesterol on phosphate uptake by human red blood cells. *FEBS Lett.* 1983; 157: 159–164. [https://doi.org/10.1016/0014-5793\(83\)81137-5](https://doi.org/10.1016/0014-5793(83)81137-5) PMID: 6862013
50. Groves JD, Tanner MJA. Glycophorin-a Facilitates the Expression of Human Band-3-Mediated Anion Transport in *Xenopus* Oocytes. *J Biol Chem.* 1992; 267: 22163–22170. Available: <http://www.jbc.org/content/267/31/22163.full.pdf> PMID: 1385395
51. Groves JD, Tanner MJ. The effects of glycophorin A on the expression of the human red cell anion transporter (band 3) in *Xenopus* oocytes. *J Memb Biol.* 1994; 140: 81–8. <https://doi.org/10.1007/BF00234488>
52. Pang AJ, Reithmeier RAF. Interaction of anion exchanger 1 and glycophorin A in human erythroleukemic K562 cells. *Biochem J.* 2009; 421: 345–356. <https://doi.org/10.1042/BJ20090345> PMID: 19438409
53. Young MT, Beckmann R, Toye AM, Tanner MJ. Red-cell glycophorin A-band 3 interactions associated with the movement of band 3 to the cell surface. *Biochem J.* 2000; 350 Pt 1: 53–60. <https://doi.org/10.1042/0264-6021:3500053>
54. Bruce LJ, Pan RJ, Cope DL, Uchikawa M, Gunn RB, Cherry RJ, et al. Altered Structure and Anion Transport Properties of Band 3 (AE1, SLC4A1) in Human Red Cells Lacking Glycophorin A. *J Biol Chem.* 2004; 279: 2414–2420. <https://doi.org/10.1074/jbc.M309826200> PMID: 14604989
55. Bruce LJ, Groves JD, Okubo Y, Thilaganathan B, Tanner MJ. Altered band 3 structure and function in glycophorin A- and B-deficient (MkMk) red blood cells. *Blood.* American Society of Hematology; 1994; 84: 916–22. Available: <http://www.ncbi.nlm.nih.gov/pubmed/8043873> PMID: 8043873
56. Bruce LJ, Ring SM, Anstee DJ, Reid ME, Wilkinson S, Tanner MJ. Changes in the blood group Wright antigens are associated with a mutation at amino acid 658 in human erythrocyte band 3: a site of interaction between band 3 and glycophorin A under certain conditions. *Blood.* 1995; 85: 541–547. [https://doi.org/10.1016/S0887-7963\(96\)80136-2](https://doi.org/10.1016/S0887-7963(96)80136-2) PMID: 7812009
57. Koldsø H, Shorthouse D, Hélie J, Sansom MSP. Lipid Clustering Correlates with Membrane Curvature as Revealed by Molecular Simulations of Complex Lipid Bilayers. *PLoS Comput Biol.* Public Library of Science; 2014; 10: e1003911. <https://doi.org/10.1371/journal.pcbi.1003911> PMID: 25340788
58. Lange Y, Cohen CM, Poznansky MJ. Transmembrane movement of cholesterol in human erythrocytes. *Proc Natl Acad Sci U S A.* National Academy of Sciences; 1977; 74: 1538–42. <https://doi.org/10.1073/PNAS.74.4.1538> PMID: 266194

59. Stansfeld PJ, Sansom MSP. From coarse grained to atomistic: A serial multiscale approach to membrane protein simulations. *J Chem Theory Comput.* American Chemical Society; 2011; 7: 1157–1166. <https://doi.org/10.1021/ct100569y> PMID: 26606363
60. Paramo T, East A, Garzón D, Ulmschneider MB, Bond PJ. Efficient characterization of protein cavities within molecular simulation trajectories: Trj-cavity. *J Chem Theory Comput.* American Chemical Society; 2014; 10: 2151–2164. <https://doi.org/10.1021/ct401098b> PMID: 26580540
61. MacKenzie KR, Prestegard JH, Engelman DM. A Transmembrane helix dimer: Structure and implications. *Science* (80-). 1997; 276: 131–133. <https://doi.org/10.1126/science.276.5309.131>
62. Petrache H, Grossfield A, MacKenzie K, Engelman D, Woolf T. Modulation of Glycophorin~A Transmembrane Helix Interactions by Lipid Bilayers: Molecular Dynamics Calculations. *J Mol Biol.* 2000; 302: 727–746. Available: <http://www.sciencedirect.com/science/article/B6WK7-45F511T-5Y/2/a268247184b35a327ef0fea5a06d6bfe> <https://doi.org/10.1006/jmbi.2000.4072> PMID: 10986130
63. Flinger N, Schleiff E. Dynamics of the glycophorin a dimer in membranes of native-like composition uncovered by coarse-grained molecular dynamics simulations. *PLoS One.* Public Library of Science; 2015; 10: e0133999. <https://doi.org/10.1371/journal.pone.0133999> PMID: 26222139
64. Ling LE, Schulz JT, Cantley LC. Characterization and purification of membrane-associated phosphatidylinositol-4-phosphate kinase from human red blood cells. *J Biol Chem.* 1989; 264: 5080–5088. Available: http://www.ncbi.nlm.nih.gov/entrez/query.fcgi?cmd=Retrieve&db=PubMed&dopt=Citation&list_uids=2538472 PMID: 2538472
65. Gascard P, T P, Lowenstein J, Cohen C. The role of inositol phospholipids in the association of band 4.1 with the human erythrocyte membrane. *Eur J Biochem.* Blackwell Publishing Ltd; 1993; 211: 671–681. <https://doi.org/10.1111/j.1432-1033.1993.tb17595.x> PMID: 8382156
66. An X, Zhang X, Debnath G, Baines AJ, Mohandas N. Phosphatidylinositol-4,5-bisphosphate (PIP2) differentially regulates the interaction of human erythrocyte protein 4.1 (4.1R) with membrane proteins. *Biochemistry.* American Chemical Society; 2006; 45: 5725–5732. <https://doi.org/10.1021/bi060015v> PMID: 16669616
67. Hanson MA, Cherezov V, Griffith MT, Roth CB, Jaakola VP, Chien EYT, et al. A Specific Cholesterol Binding Site Is Established by the 2.8 Å Structure of the Human β 2-Adrenergic Receptor. *Structure.* 2008; 16: 897–905. <https://doi.org/10.1016/j.str.2008.05.001> PMID: 18547522
68. Zocher M, Zhang C, Rasmussen SGF, Kobilka BK, Muller DJ. Cholesterol increases kinetic, energetic, and mechanical stability of the human 2-adrenergic receptor. *Proc Natl Acad Sci.* 2012; 109: E3463–E3472. <https://doi.org/10.1073/pnas.1210373109> PMID: 23151510
69. Mühlebach T, Cherry RJ. Influence of Cholesterol on the Rotation and Self-Association of Band 3 in the Human Erythrocyte Membrane. *Biochemistry.* American Chemical Society; 1982; 21: 4225–4228. <https://doi.org/10.1021/bi00261a006> PMID: 7126539
70. Fantini J, Barrantes FJ. How cholesterol interacts with membrane proteins: An exploration of cholesterol-binding sites including CRAC, CARC, and tilted domains. *Front Physiol.* 2013; 4 FEB: 1. <https://doi.org/10.3389/fphys.2013.00001>
71. Mankelov TJ, Satchwell TJ, Burton NM. Refined views of multi-protein complexes in the erythrocyte membrane. *Blood Cells, Mol Dis.* 2012; 49: 1–10. <https://doi.org/10.1016/j.bcmd.2012.03.001> PMID: 22465511
72. Williamson RC, Teye AM. Glycophorin A: Band 3 aid. *Blood Cells, Mol Dis.* 2008; 41: 35–43. <https://doi.org/10.1016/j.bcmd.2008.01.001> PMID: 18304844
73. Telen MJ, Chasis JA. Relationship of the human erythrocyte Wrb antigen to an interaction between glycophorin A and band 3. *Blood.* 1990; 76: 842–848. Available: <http://www.ncbi.nlm.nih.gov/pubmed/2383660> PMID: 2383660
74. Hassoun H, Hanada T, Lutchman M, Sahr KE, Palek J, Hanspal M, et al. Complete deficiency of glycophorin A in red blood cells from mice with targeted inactivation of the band 3 (AE1) gene. *Blood.* 1998; 91: 2146–2151. [https://doi.org/10.1016/S0887-7963\(99\)80106-0](https://doi.org/10.1016/S0887-7963(99)80106-0) PMID: 9490702
75. Nigg EA, Cherry RJ, Bron C, Girardet M. Band 3-Glycophorin A Association in Erythrocyte Membranes Demonstrated by Combining Protein Diffusion Measurements with Antibody-Induced Cross-Linking. *Biochemistry.* 1980; 19: 1887–1893. <https://doi.org/10.1021/bi00550a024> PMID: 7378378
76. Che A, Cherry RJ. Loss of rotational mobility of band 3 proteins in human erythrocyte membranes induced by antibodies to glycophorin A. *Biophys J.* Elsevier; 1995; 68: 1881–1887. [https://doi.org/10.1016/S0006-3495\(95\)80365-6](https://doi.org/10.1016/S0006-3495(95)80365-6) PMID: 7612830
77. Knowles DW, Chasis JA, Evans EA, Mohandas N. Cooperative action between band 3 and glycophorin A in human erythrocytes: immobilization of band 3 induced by antibodies to glycophorin A. *Biophys J.* 1994; 66: 1726–1732. [https://doi.org/10.1016/S0006-3495\(94\)80965-8](https://doi.org/10.1016/S0006-3495(94)80965-8) PMID: 8061221

78. Giger K, Habib I, Ritchie K, Low PS. Diffusion of glycophorin A in human erythrocytes. *Biochim Biophys Acta—Biomembr.* NIH Public Access; 2016; 1858: 2839–2845. <https://doi.org/10.1016/j.bbmem.2016.08.012> PMID: 27580023
79. Young MT, Tanner MJA. Distinct regions of human glycophorin A enhance human red cell anion exchanger (band 3; AE1) transport function and surface trafficking. *J Biol Chem. American Society for Biochemistry and Molecular Biology*; 2003; 278: 32954–32961. <https://doi.org/10.1074/jbc.M302527200> PMID: 12813056
80. Tanphaichitr VS, Sumboonnanda A, Ideguchi H, Shayakul C, Brugnara C, Takao M, et al. Novel AE1 mutations in recessive distal renal tubular acidosis. Loss- of-function is rescued by glycophorin A. *J Clin Invest. The American Society for Clinical Investigation*; 1998; 102: 2173–2179. <https://doi.org/10.1172/JCI4836> PMID: 9854053
81. Jensen D, Schekman R. COPII-mediated vesicle formation at a glance. *J Cell Sci.* 2011; 124: 1–4. <https://doi.org/10.1242/jcs.069773> PMID: 21172817
82. Fowler PW, Sansom MSP, Reithmeier RAF. Effect of the Southeast Asian Ovalocytosis Deletion on the Conformational Dynamics of Signal-Anchor Transmembrane Segment 1 of Red Cell Anion Exchanger 1 (AE1, Band 3, or SLC4A1). *Biochemistry. American Chemical Society*; 2017; 56: 712–722. <https://doi.org/10.1021/acs.biochem.6b00966> PMID: 28068080
83. Javanainen M, Martinez-Seara H, Vattulainen I. Excessive aggregation of membrane proteins in the Martini model. Papaleo E, editor. *PLoS One. Public Library of Science*; 2017; 12: e0187936. <https://doi.org/10.1371/journal.pone.0187936> PMID: 29131844
84. Hedger G, Shorthouse D, Koldsø H, Sansom MSP. Free Energy Landscape of Lipid Interactions with Regulatory Binding Sites on the Transmembrane Domain of the EGF Receptor. *J Phys Chem B. American Chemical Society*; 2016; 120: 8154–8163. <https://doi.org/10.1021/acs.jpcc.6b01387> PMID: 27109430
85. Naughton FB, Kalli AC, Sansom MSP. Modes of Interaction of Pleckstrin Homology Domains with Membranes: Toward a Computational Biochemistry of Membrane Recognition. *J Mol Biol. Academic Press*; 2018; 430: 372–388. <https://doi.org/10.1016/j.jmb.2017.12.011> PMID: 29273202
86. Sengupta D, Marrink SJ. Lipid-mediated interactions tune the association of glycophorin A helix and its disruptive mutants in membranes. *Phys Chem Chem Phys.* 2010; 12: 12987. <https://doi.org/10.1039/c0cp00101e> PMID: 20733990
87. De Jong DH, Singh G, Bennett WFD, Arnarez C, Wassenaar TA, Schäfer L V., et al. Improved parameters for the martini coarse-grained protein force field. *J Chem Theory Comput. American Chemical Society*; 2013; 9: 687–697. <https://doi.org/10.1021/ct300646g> PMID: 26589065
88. Marrink SJ, Risselada HJ, Yefimov S, Tieleman DP, De Vries AH. The MARTINI force field: Coarse grained model for biomolecular simulations. *J Phys Chem B. American Chemical Society*; 2007; 111: 7812–7824. <https://doi.org/10.1021/jp071097f> PMID: 17569554
89. Van Der Spoel D, Lindahl E, Hess B, Groenhof G, Mark AE, Berendsen HJC. GROMACS: Fast, flexible, and free. *J Comput Chem.* 2005; 26: 1701–1718. <https://doi.org/10.1002/jcc.20291> PMID: 16211538
90. Fiser A, Šali A. Generation and refinement of homology-based protein structure models. *Meths Enzym.* 2003; 374: 461–491. [https://doi.org/10.1016/S0076-6879\(03\)74020-8](https://doi.org/10.1016/S0076-6879(03)74020-8)
91. Sali A. Comparative protein modeling by satisfaction of spatial restraints. *Mol Med Today.* 1995; 1: 270–277. [https://doi.org/10.1016/S1357-4310\(95\)91170-7](https://doi.org/10.1016/S1357-4310(95)91170-7) PMID: 9415161
92. Bussi G, Donadio D, Parrinello M. Canonical sampling through velocity rescaling. *J Chem Phys.* 2007; 126: 14101. <https://doi.org/10.1063/1.2408420> PMID: 17212484
93. Parrinello A. M. R. Polymorphic transitions in single crystals: A new molecular dynamics method. *J Appl Phys. AIP*; 1981; 52: 7182–7190. Available: <http://link.aip.org/link/?JAP/52/7182/1>
94. Darden T, York D, Pedersen L. Particle mesh Ewald: An N-log(N) method for Ewald sums in large systems. *J Chem Phys.* 1993; 98: 10089–10092. <https://doi.org/10.1063/1.464397>
95. Hess B, Bekker H, Berendsen HJC, Fraaije J. LINC: A Linear Constant Solver for Molecular Simulations. *J Comput Chem.* 1997; 18: 1463–1472. Available: citeulike-article-id:2139559
96. Stansfeld PJ, Jefferys EE, Sansom MSP. Multiscale simulations reveal conserved patterns of lipid interactions with aquaporins. *Structure.* 2013; 21: 810–819. <https://doi.org/10.1016/j.str.2013.03.005> PMID: 23602661
97. Schmidt MR, Stansfeld PJ, Tucker SJ, Sansom MSP. Simulation-based prediction of phosphatidylinositol 4,5-bisphosphate binding to an ion channel. *Biochemistry. American Chemical Society*; 2013; 52: 279–281. <https://doi.org/10.1021/bi301350s> PMID: 23270460
98. Hedger G, Rouse SL, Domański J, Chavent M, Koldsø H, Sansom MSP. Lipid-Loving ANTs: Molecular Simulations of Cardiolipin Interactions and the Organization of the Adenine Nucleotide Translocase in Model Mitochondrial Membranes. *Biochemistry. American Chemical Society*; 2016; 55: 6238–6249. <https://doi.org/10.1021/acs.biochem.6b00751> PMID: 27786441